Autophagy

Volume 11 - Issue 11 - November 2015

Editor-in-Chief
Daniel J. Klionsky
University of Michigan

Taylor & Francis
Taylor & Francis Group

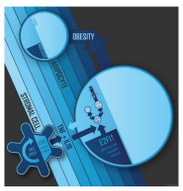

Autophagy

ISSN: (Print) (Online) Journal homepage: https://www.tandfonline.com/loi/kaup20

Inactivation of the *Caenorhabditis elegans* RNF-5 E3 ligase promotes IRE-1-independent ER functions

Limor Broday , Orit Adir , Ulrike Bening-Abu-Shach , Shir Arbib & Sivan Henis-Korenblit

To cite this article: Limor Broday , Orit Adir , Ulrike Bening-Abu-Shach , Shir Arbib & Sivan Henis-Korenblit (2020): Inactivation of the *Caenorhabditis elegans* RNF-5 E3 ligase promotes IRE-1-independent ER functions, Autophagy, DOI: 10.1080/15548627.2020.1827778

To link to this article: https://doi.org/10.1080/15548627.2020.1827778

Publisher: Taylor & Francis & Informa UK Limited, trading as Taylor & Francis Group

Journal: *Autophagy*

DOI: 10.1080/15548627.2020.1827778

Inactivation of the *Caenorhabditis elegans* RNF-5 E3 ligase promotes IRE-1-independent ER functions

Orit Adir[1], Ulrike Bening-Abu-Shach[1], Shir Arbib[2], Sivan Henis-Korenblit[2] and Limor Broday[1]

[1]Department of Cell and Developmental Biology, School of Medicine, Tel Aviv University, Tel Aviv, Israel.
[2]The Mina and Everard Goodman Faculty of Life Sciences, Bar-Ilan University, Ramat-Gan, Israel.

Contact: broday@tauex.tau.ac.il

Abstract

RNF5 is implicated in ERAD and in negative regulation of macroautophagy/autophagy. To better understand the function of RNF-5 under ER-stress conditions, we studied the ability of *Caenorhabditis elegans rnf-5(tm794)* mutant animals to cope with stress in the background of impaired UPR machinery. We demonstrate that downregulation of RNF-5 decreased sensitivity to tunicamycin both in wild type and in an *ire-1* mutant. Double-mutant *rnf-5;ire-1* animals showed increased starvation resistance and extended lifespan when compared to the *ire-1* mutant. This partial rescue of *ire-1* required functional autophagy. Downregulation of RNF-5 rescued ER maturation defects and protein secretion of a DAF-28::GFP intestinal reporter in the *ire-1* background. Proteomics and functional studies revealed an increase in lysosomal protease levels, in the frequency of intestinal lysosomes, and in lysosomal protease activity in *rnf-5(tm794)* animals. Together, these data suggest that RNF-5 is a negative regulator of ER stress, and that inactivation of RNF-5 promotes IRE-1-independent elevation of ER capacity.

Abbreviations

ATG: autophagy; ER: endoplasmic reticulum; ERAD: ER-associated protein degradation; RNF5: RING finger protein 5; UPR: unfolded protein response; WT: wild-type

Key Words

autophagy, *C. elegans,* endoplasmic reticulum, IRE1, lysosome, RMA1, RNF5

Introduction

Endoplasmic reticulum (ER) stress is caused primarily by an increase in misfolded protein load in the ER. The unfolded protein response (UPR) [1,2] and ER-associated degradation (ERAD) [3] are key interconnected quality-control pathways that sense and respond to ER stress and act in coordination to resolve the stress in this organelle [2,4]. One hallmark of the UPR is the activation of a set of stress-regulated transcription factors, that transcribe genes that promote protein folding (via expression of ER-resident protein chaperones), as well as protein degradation (via expression of proteins related to proteasome function, ERAD and autophagy)[2,4]. Together, the UPR orchestrates and coordinates between quality-control pathways that sense and respond to ER stress. The main sensor of the UPR is the ER membrane protein ERN1/IRE1, a type-I transmembrane ER-resident protein highly conserved along evolution [5,6]. In *C. elegans* the UPR system maintains ER homeostasis during development and under stress [7,8]. In normal growth conditions *ire-1* mutant animals develop slowly [7,8], exhibit impaired secretory protein metabolism[9], have a shortened lifespan [10] and fail to recover from starvation-induced developmental arrest [11].

Macroautophagy/autophagy is an evolutionarily conserved process of degradation of cytoplasmic components by the lysosome, including organelles and long-lived misfolded proteins. This process enables the recycling of amino acids, carbohydrates, lipids, and nucleotides as well as the removal of aberrant macromolecules and organelles. In this way, autophagy contributes to the health and functionality of cells and organisms [12,13]. Autophagy involves the formation of a double-membrane organelles which transport intracellular components to the lysosome for degradation [12,13]. More than 30 autophagy-related (*ATG*) genes have been identified to be required for the process of autophagy in *S. cerevisiae*, most of which are conserved from yeast to mammals [14,15]. Autophagy is induced by the activation of a serine/threonine protein kinase complex. Nucleation of the phagophore requires the class III phosphatidylinositol 3-kinase Vps34-containing complex, which includes Vps30/Atg6/BEC-1, Vps34/VPS-34, Vps15/VPS-15, Atg14/EPG-8 and Atg38. Expansion of the phagophore in yeast requires two ubiquitin-like conjugation systems resulting in the ubiquitin-like protein Atg8 (in *C. elegans* LGG-1 and LGG-2) to be conjugated to phosphatidylethanolamine (PE), with the aid of Atg4 cysteine proteases,

the E1-like activating enzyme Atg7 and the E2-like conjugating enzyme, Atg3 [14] [15]. Orthologs to all of these components exist in *C. elegans* [16]. While autophagy occurs at a basal constitutive level to mediate global turnover of cytoplasmic materials [17], it can be further induced in response to nutrient deprivation and prevents amino acid insufficiency as well as energy production, both of which are essential for survival and adaptation to starvation [18,19]. Autophagy is also induced by other stresses, such as ER stress [20-25]. In this case, autophagy induction may be used to eliminate misfolded proteins that exceed the ERAD capacity for their clearance [26,27].

The ERN1/IRE1-MAPK/JNK pathway has been demonstrated to promote autophagy activation following ER stress [21]. Specifically, activated ERN1/IRE1α can result in MAPK/JNK-mediated phosphorylation of BCL2, thereby disrupting the BECN1-BCL2 inhibitory complex [28-30]. This frees BECN1 to form the PIK3C3/Vps34-BECN1 complex to promote vesicle nucleation, a critical step in the generation of the phagophore [31,32] . In addition, activated ERN1 removes an inhibitory intron from the *XBP1* transcript, generating the transcription factor spliced XBP1, which promotes the transcription of BECN1 [33]. Neuronal XBP-1 activates intestinal lysosomes to improve proteostasis in *C. elegans* [34]. Furthermore, additional stages in the process of autophagy such as autophagy induction, vesicle nucleation, and elongation are regulated by UPR components as well as by Ca^{2+} signaling [35] [36].

RNF5 is a highly conserved E3 ubiquitin ligase implicated in clearance of misfolded proteins from the ER through the ERAD pathway [37-39]. One of the most established substrates of the mammalian RNF5 is the ERAD substrate CFTRΔF508, a mutant form of CFTR (CF transmembrane conductance regulator) [37,40-42]. RNF5 has been demonstrated to regulate glutamine carrier proteins, which are aberrantly folded following chemotherapy-induced ER stress [43]. RNF5 mediates viral-triggered ubiquitination and degradation of STING1/MITA [44] and MAVS/VISA [45] acting as a negative regulator of type I IFNs induction during cellular antiviral response [45]. Importantly, a recent study has demonstrated that *Rnf5*-deleted mice exhibit attenuated activation of key UPR components but increased expression of ER-stress markers in the intestine, including the ER chaperone BIP [46]. A cDNA library screen using a yeast-based functional assay for ATG4B inhibitors identified RNF5 and highlighted its role in the negative regulation of autophagy [47]. The study demonstrated that RNF5 functions to limit basal levels of autophagy in cultured cells, mice and *C. elegans* by ubiquitination and degradation of a membrane-associated pool of ATG4B and subsequent control of LC3 processing [47]. In *C. elegans*, RNF-5 regulates the molting process through regulation of the dense body protein UNC-95 [48,49] and modulates cell migration similarly to the mammalian ortholog [50,51]. We have shown that the role of RNF5 in autophagy is conserved along evolution and downregulation of RNF-5 in *C. elegans* increases

autophagy [47]. In this study, we investigated the molecular mechanisms by which RNF-5 contributes to the maintenance of ER homeostasis. We show that downregulation of RNF-5 increased ER stress resistance and partially rescued *ire-1* mutant animals in an autophagy-dependent manner.

Results

Increased ER stress resistance of* rnf-5(tm794) *mutant animals

We have previously demonstrated that RNF-5 is a negative regulator of autophagy both in *C. elegans* and mammalian systems through its regulation of ATG4B [47]. In order to examine if the increase in autophagy induced by RNF-5 depletion also enables animals to better cope with ER stress, we examined if downregulation of RNF-5 affects sensitivity to ER stress. Growing *rnf-5(tm794)* deletion mutant in media containing the ER stress inducer tunicamycin resulted in a better ability of the mutant animals to develop to L4 larvae and adults when compared to wild type animals. This rescue was limited to mild ER stress (tunicamycin ≤2 µg/ml) as *rnf-5(tm794)* animals exhibited similar sensitivity as wild type animals in tunicamycin concentrations of ≥3 µg/ml resulting in developmental arrest (Fig. 1A).

To examine the relation between the increased ER stress resistance of *rnf-5(tm794)* to the known role of RNF-5 in autophagy, we examined sensitivity to 1.5 µg/ml tunicamycin following down-regulation of autophagy genes by RNAi. Both wild-type and *rnf-5(tm794)* animals became more sensitive to tunicamycin following *atg-4.1*, *atg-4.2*, *bec-1*, *atg-7* and *lgg-1* RNAi (Fig. 1B). There was no inhibition of growth on solvent DMSO RNAi plates (Fig. S1). In general, *rnf-5(tm794)* showed higher resistance compared to wild type in most of the conditions, but when lgg-1 was downregulated or both *atg-4.1* (ortholog to the human ATG4A and ATG4B) and *atg-4.2* (ortholog to the human ATG4C) were co-downregulated, *rnf-5(tm794)* animals lost their resistance and showed sensitivity similar to wild-type animals. This data suggests that downregulation of RNF5 increase resistance to ER stress depends on functional autophagy.

rnf-5 *knockout partially rescues the ire-1 mutant animals with impaired UPR*

To elucidate the association between elevated ER stress resistance and the unfolded protein response (UPR) in *rnf-5(tm794)* mutant animals we next analyzed mutants with impaired UPR. The IRE-1 stress sensor plays a key role in maintaining ER homeostasis by initiating the signaling through the IRE-1/XBP-1 arm of the UPR and is required for cell-survival after tunicamycin-induced ER-stress [7]. We examined the ability of *rnf-5;ire-1* double mutants to develop in the presence of tunicamycin. While 70±2.5% of

ire-1(v33) mutant animals developed to L4 and adults in DMSO control plates, only 60±3.5% developed in mild ER stress (1 µg/ml tunicamycin). In this concentration of tunicamycin 77±2.3% of WT animals developed normally. Double mutant *rnf-5(tm794);ire-1(v33)* rescued the developmental arrest in DMSO control plates as well as the sensitivity of *ire-1(v33)* to 1 µg/ml tunicamycin to 81±2.4% and 72±3.1% respectively (Fig. 1C and Table S1).

Similarly, we examined the ability of *rnf-5; ire-1* double mutants to recover from a prolonged heat shock, which is associated with proteostasis stress in various cellular organelles including the ER. We performed heat shock experiments on WT, *rnf-5* and *ire-1* single mutant and *ire-1;rnf-5* double mutants (Fig. S2). Surprisingly, under acute heat shock conditions (37°C for 5 h 30 min), we found that *rnf-5* mutant animals showed a trend of higher sensitivity to heat shock compared to WT. We hypothesize that the basal high levels of autophagy in *rnf-5* mutant animals along with the additional induction of autophagy by heat shock conditions probably resulted in excessive autophagy, leading to lower thermo-resistance. In contrast, *ire-1; rnf-5* double mutants showed increased thermo-resistance compared to single mutants and to WT animals. This result highlights the benefits provided by *rnf-5* depletion in *ire-1* deficient animals, whose ERAD and lysosome functions are compromised.

We next assayed another stress condition, the ability of L1 animals to complete normal development when returned to food following starvation. L1 larvae reversibly arrest development in response to starvation [52]. This starvation-induced quiescence increases stress resistance [11]. Different mutants exhibit difference in starvation survival, for example *daf-2* mutants survive longer in starvation than wild type [53,54] and IRE-1 is essential for recovery from L1 arrest [11]. While wild type and *rnf-5(tm794)* animals resumed development after 21.8±0.2 and 23.3±0.2 days of starvation respectively, *ire-1(v33)* mutant animals accumulated dead cell vacuoles (Fig. 2E) and could develop to adults only after maximum 10.2±0.5 days of starvation. Interestingly, *rnf-5(tm794);ire-1(v33)* double mutants displayed a dramatically improved survival of 15.2±0.3 days (Fig. 2A and Table S2). To determine the requirement for autophagy in this process we next performed L1 starvation assay in the background of *atg-3(bp412),* a hypomorphic *atg-3* allele [55,56]. ATG-3 is an ortholog of human ATG3 and is predicted to have Atg8 ligase activity [57,58]. Autophagy is required to resist starvation [59] and indeed the survival of *atg-3(bp412)* animals was similar to *ire-1(v33).* In contrast to *ire-1(v33),* double mutant with *rnf-5(tm794)* did not improve the *atg-3(bp412)* phenotype suggesting that functional autophagy is required for rescuing the starved L1s (Fig. 2B). Double and triple mutants *ire-1(v33); atg-3(bp412)* and *ire-1(v33); atg-3(bp412);rnf-5(tm794)* developed to adults similarly to *ire-1(v33)* (Fig. 2C-D). When analyzed under ER stress conditions the double mutant *atg-3(bp412);rnf-5(tm794)* did not improve the weak sensitivity of

atg-3(bp412) to mild ER stress (tunicamycin ≤2 µg/ml) (Fig. S3). We conclude that autophagy contributes to the rescue of *ire-1;rnf-5* double mutant ability to overcome L1 starvation.

rnf-5 *knockout increases the lifespan of* ire-1 *mutant animals*

The lifespan of *ire-1(v33)* animals is much shorter (9.4±0.3 days) when compared to wild type and *rnf-5(tm794)* (20±0.5 and 21.1±0.5 days, respectively), but in double mutant *rnf-5(tm794);ire-1(v33)* the lifespan was extended to 12.5±0.3 days (Fig. 3A and Table S3). Similarly to the starvation assay, also the lifespan of *atg-3(bp412)* was shorter while double mutant *atg-3(bp412);rnf-5(tm794)* did not rescue the short lifespan of *atg-3* mutant animals (13.9±0.2 and 14.1±0.2 days respectively; Fig. 3B). In addition, downregulation of autophagy did not further decrease *ire-1* mutant lifespan (Fig. 3C). Importantly, we find that autophagy is required for the extension of *ire-1* mutant lifespan by downregulation of RNF-5 as the triple mutant *atg-3(bp412);rnf-5(tm794);ire-1(v33)* had a shorter lifespan (10.5±0.3 days) when compared to *rnf-5;ire-1* double mutant (Fig. 3D). In summary, we conclude that the knockout of *rnf-5* extends the lifespan of *ire-1* mutant worms in an *atg-3* dependent manner.

Knockout of* rnf-5 *improved ER function in* ire-1 *mutant animals

IRE-1 plays a central role in secretory protein metabolism also under normal growth conditions [9]. To better understand how downregulation of RNF-5 affects protein secretion in *ire*-1 mutant animals we analyzed the *daf-28p*::DAF-28::GFP reporter [60,61]. DAF-28 is one of the worm insulins. In wild-type animals DAF-28::GFP is produced in several anterior sensory neurons and in the posterior intestine and secreted to the coelom. The coelomocytes uptake and remove the secreted protein from the body cavity. In wild-type animals, a GFP signal is detected in anterior sensory neurons, the posterior intestine and in coelomocytes. There is only a weak signal in the body cavity since the reporter is rapidly removed by the coelomocyte cells following its secretion. As previously described [9], in *ire-1* mutant worms the reporter accumulates in the producing cells leading to relatively high signal in the anterior sensory neurons and posterior intestine. In these animals, the DAF-28::GFP reporter is not secreted from the producing cells due to abnormal ER function in *ire-1* mutant and therefore there is only a low signal in the body cavity. However, we find that in *ire-1;rnf-5* double mutants more than 80% of the animals had DAF-28::GFP fluorescence in the body cavity (Fig. 4A-B) suggesting an increased secretion of the DAF-28::GFP from the producing cells, but no clearance by the coelomocytes (coelomocytes are present in *ire-1* mutants, but are dysfunctional [9]). We could not detect a difference in the fluorescence in the sensory neurons, which remained high in *rnf-5; ire-1* double mutants (Fig. 4A, 4C), but detected a

significant decrease in fluorescence in the posterior intestine (Fig. 4A, 4D) and an increase in the fluorescence in the body cavity in *ire-1;rnf-5* animals (Fig. 4A, 4B and 4E). Altogether, this suggest that downregulation of RNF-5 partially rescues the secretory ER activity at least in the DAF-28::GFP intestinal producing cells, allowing secretion of the reporter from these cells. However the rescue is partial as secretion of the reporter from the neurons was not restored, and the coelomocytes of *ire-1;rnf-5* animals remained non-functional. A similar rescue pattern (i.e. rescue of secretion of the reporter from the intestine producing cells, but not from the producing neuronal cells, and lack of rescue of coelomocyte activity) has been observed in the insulin/IGF-1 receptor *daf-2* mutants [62]. Interestingly, this implies that RNF-5 probably acts in a cell non-autonomous manner through an hormonal signaling pathway to enhance secretion in the intestine, since a transcriptional *rnf-5p*::mCherry reporter was expressed in head and tail neurons and in the epidermis but not in intestinal cells (Fig. S4).

Increased levels of lysosomal proteases in* rnf-5(tm794) *mutant animals

To identify downstream elements regulated by RNF-5, we performed a quantitative proteomic profiling of wild type and *rnf-5(tm794)* mutant animals under mild ER stress induced by 1µg/ml tunicamycin. Our analysis identified 44 proteins with higher levels in *rnf-5(tm794)* animals compared to wild-type animals and 4 proteins with lower levels (Fig. 5A and Table S3). Functional annotation (DAVID) showed enrichment in two main clusters: hydrolases ($p<0.00001$) and RNA helicases ($p<0.003$). We identified an increase in the levels of 19 hydrolases including cysteine proteases, aspartic peptidases, additional lysosomal hydrolases and oxidoreductases. Network of protein-protein interactions in the two clusters was identified using STRING [63] (Fig. 5A). Because many of these hydrolases were shown to be involved in lysosomal function and autophagy also in *C. elegans* [34] it is possible that RNF-5 regulates the levels of these components through a lysosomal or authophagy central regulator and therefore their levels are increased in *rnf-5(tm794)* mutant animals. We have previously showed that RNF-5 regulates the ATG4B cysteine protease [47] and this new data suggest that RNF-5 may regulate a larger family of proteases. To examine the lysosomes in *rnf-5(tm794)* mutant animals we stained animals with LysoTracker Red DND-99 and analyzed the region of the anterior intestine, immediately posterior to the pharyngeal-intestinal valve. We detected more lysosomes in *rnf-5(tm794)* which in most cases did not co-localize with autophagosomes marked by GFP::LGG-1 reporter (Fig. 5B). Quantification of the lysosomes showed significant increase in lysosome number as well as significant decrease in lysosome size suggesting an increase in newly formed lysosomes in *rnf-5(tm794)* mutant animals when compared to WT. Quantification of the lysosomes in *ire-1(v33)* revealed weaker staining and smaller number of lysosomes

that was rescued in the double mutant *rnf-5(tm794); ire-1(v33).* The size of the lysosomes was not significantly different from WT in all strains except *rnf-5(tm794)* with significantly smaller lysosomes (Fig. 5C-D). Finally, to examine the effect of RNF-5 depletion on lysosomal activity we stained the worms with Magic Red cathepsin B substrate. This substrate produces fluorescence in the intestine upon cleavage by lysosomal proteases. As expected, *rnf-5* mutant animals exhibited higher lysosomal activity while *ire-1* mutant animals showed low activity as evidenced by reduced fluorescence. Importantly, the cathepsin B activity was increased in *ire-1; rnf-5* double mutants compared to *ire-1* single mutants mainly in the anterior and posterior intestine, but not to the level of WT (Fig. S5). Altogether, these experiments prove that *rnf-5* deficiency modulates lysosome biogenesis and increases lysosomal protease activity as predicted by our proteomics data.

Discussion

In this study we show that downregulation of the conserved E3 ligase RNF-5 enhances *C. elegans* resistance to the ER toxin tunicamycin and improves the physiology of IRE-1-compromised animals. Given the well-established role of RNF-5 in limiting autophagy, we examined whether these benefits could be mediated by the autophagy-enhancing effects of RNF-5 depletion. Consistent with this hypothesis, we found that RNF-5 depletion was less beneficial in improving the physiology of *ire-1* mutants in a starvation recovery assay and in a lifespan assay, in the background of the autophagy hypo-morph *atg-3(bp412).* Likewise, RNF-5 depletion was less beneficial in improving tunicamycin resistance in animals treated with RNAi of autophagy genes. Interestingly, RNF-5 depletion was still beneficial in improving tunicamycin resistance in animals treated with RNAi against *atg-4.1* and *atg-4.2* individually, or upon silencing *bec-1* and *atg-7*. This tunicamycin resistance may be due to residual autophagic activity in these animals due to differences in RNAi efficiency. Since combination of *atg-4.1* and *atg-4.2* had the strongest affect, it could be that RNF-5 depletion also improves the resistance of the animals to tunicamycin in an ATG4-dependent but autophagy-independent mechanism. These findings are consistent with the established role of RNF5 as an ATG4B regulator [47] and with the broad implications of a variety of *ATG* gene functions in different membrane-trafficking and signaling pathways [64]. Interestingly, when compared to wild-type animals, knockout of *rnf-5* was not beneficial in all the conditions tested. Specifically, *rnf-5* inactivation improved resistance only to low concentrations of tunicamycin and did not affect the resistance to high concentrations of this drug. Likewise, it extended the lifespan and improved the recovery of L1 larvae from starvation in *ire-1* deficient animals, with only a slight effect on wild-type animals. Whereas *rnf-5* depletion significantly improved the recovery of *ire-*

1(-) animals from prolonged heat stress, it actually showed sensitivity to heat stress. We hypothesize that the underlying cause for these differential effects of *rnf-5* depletion may reflect the characteristics double-edged sword activity of autophagy [65]. For example, in conditions where autophagy levels are naturally low (for example under low concentrations of tunicamycin or in aging and L1-arrested *ire-1*-deficient animals), the *rnf-5(-)* mediated increase in autophagy levels may be beneficial for the organism. In contrast in conditions where autophagy levels are increased (for example when exposed to high concentrations of tunicamycin or in aging or L1-arrested wild-type animals), a further increase in autophagy levels may not have an added value for the organism. Furthermore, having too much autophagy may even harm the animals, as in the case of *rnf-5*-deficient animals exposed to heat stress. Consistent with this interpretation, too much or too little autophagy reduces recovery from L1 arrest [52]. Likewise, it has been shown that excessive autophagy in the pharyngeal muscles causes damage to the pharynx and result in animal death [59].

We demonstrated that downregulation of RNF-5 increased survival of *ire-1* mutant animals following starvation and extended *ire-1* mutant lifespan if the autophagy system remains intact. Our current observations together with our previous study [47] suggest that the increased autophagy levels following RNF5 downregulation is independent of the ERN1 UPR system. Using the DAF-28::GFP model for protein secretion we demonstrated that downregulation of RNF-5 rescued intestinal protein secretion in *ire-1* mutant animals. Interestingly, analysis of the transcriptional *rnf-5* reporter strain suggests that RNF-5 is expressed in neurons, rather than in the intestine. This suggests that RNF-5 acts cell non-autonomously to promote ER function in the intestine, and possibly in additional tissues. Accordingly, RNF-5 depletion increased Cathepsin B activity throughout the organism, primarily in the intestine. This suggests that RNF-5 may be involved in a hormonal signaling pathway that regulates autophagy and lysosomal activity. This pathway is yet to be identified in future studies. Interestingly, RNA-seq analysis of intestines of animals expressing neuronal XBP-1, has recently identified upregulation of the same lysosomal genes [34], suggesting that RNF-5 acts in a parallel pathway potentially compensating for IRE-1 deficiency.

Secretory proteins are critical for cell-to-cell communication within an organism and between organisms. ER stress conditions, induced by toxins such as tunicamycin, or by defects in the ER homeostasis stress response pathway, perturb ER function, and consequently perturb secretory protein metabolism [9]. These in turn may account for the reduced survival of ER-stressed animals under different challenging conditions. Here we demonstrate that depletion of *rnf-5* partially restores protein secretion in *ire-1*-deficient animals, improving their resistance to ER stress and their longevity. We

attribute these improvements to two distinct mechanisms, that most likely act in parallel and complement each other. First, blocking ER secretion per se is sufficient to cause ER stress and activate the ER-UPR [66]. Thus, a relive in protein secretion can by itself reduce the load on the ER and thus promote ER homeostasis and function. Second, the improved physiology of the animals may be due to restoration of hormonal signals that rely on functional protein secretion. Accordingly, longevity and activation of the ER stress response, both involve secreted proteins that function in a hormonal like fashion.

The results from the proteomics screen suggest that RNF-5 depletion increases the level of a large family of lysosomal proteases. The lysosome is the terminal organelle for the autophagic cargo. Interestingly, lysosomes function decline with age in a lifespan and proteostasis-limiting manner [55,67,68]. We analyzed lysosome size and number in the anterior intestine using lysotracker. We measured significant increase in the number of lysosomes and decrease in their size in *rnf-5(tm794)* animals. Furthermore, we found that there is no colocalization between the lysosomes and the GFP::LGG-1 autophagosomes, supporting an increase in autophagosome formation in *rnf-5(tm794)* animals as well as increase in nascent lysosome formation or budding . In *ire-1* mutants we observed weak staining of the lysosomes suggesting increased lysosomal pH/impaired lysosome acidification or abnormal retention properties inside the organelle. This inefficient staining was rescued in the double mutant *rnf-5(tm794); ire-1(v33).* We confirmed that *rnf-5* mutant animals have higher lysosomal protease activity as predicted by the proteomics data. In addition, the proteomic screen identified an increase in the level of several RNA helicases including GLH-1, GLH-2 and H20J04.4 which encode DEAD-box RNA helicases. GLH-1 and GLH-2 have known roles in germline development [69]. In mammals, a family of DExD/H box RNA helicases recruit the STING1/MITA and MAVS/VISA adaptors, that are RNF5 substrates [44,45], to activate the transcription factor NFKB/NF-κB leading to transcriptional induction of the genes encoding type I IFNs and other antiviral effectors [70]. Thus, RNF-5 may also play a role in basal defense mechanisms against pathogens. Consistent with this possibility, one of the enriched proteins upon RNF-5 depletion is the innate immunity-related protein IRG-7(F40F4.6) (Table S4)[71]. Interestingly, there was a major decrease in the levels of Aurora-A kinase AIR-1 (Table S4, red) in *rnf-5(tm794)* animals when compared to wild-type. Autophagy was shown to increase following downregulation of AURKA/Aurora-A kinase [72] but the functional association between RNF-5 and AIR-1 is still unknown.

In summary, we present evidence suggesting that RNF-5 negatively regulates lysosomal proteases levels. Downregulation of RNF-5 elevated lysosomal number and function and animal resistance to stress probably by enhancing lysosome capacity and by this also ER stress resistance. Our findings may

contribute to therapeutic developments for lysosomal storage disorders and late-onset neurodegenerative diseases like Alzheimer and Parkinson diseases.

Materials and Methods

Strains

Strains were cultured and maintained at 20° unless specified otherwise. The following strains were used in this study: *rnf-5(tm794), ire-1(v33), ire-1(ok799), atg-3(bp412)*, NX169 [*ire-1(v33)*II;*rnf-5(tm794)*III], VB1605 svIs69[pdaf-28::daf-28::gfp], SHK11 *ire-1(ok799)*; svIs69[Pdaf-28::DAF-28::GFP], SHK495 *ire-1(ok799)II; rnf-5(tm794*); svIs69 [Pdaf-28::daf-28::gfp]. The *rnf-5(tm794)* deletion allele is a probable null allele and has a 647-bp deletion in exon 2 that results in a frameshift and a stop codon after 37 amino acids [50,73].

Tunicamycin Sensitivity Assay

Tunicamycin (Sigma, T7765) plates were prepared by spreading tunicamycin on NGM (51 mM NaCl, 2.5 g/L Bacto Tryptone, 17 g/L Bacto Agar, 5 µg/ml cholesterol, 25 mM KH_2PO_4/K_2HPO_4, pH 6, 1 mM $MgSO_4$, 1 mM $CaCl_2$) plates, and allowing plates to dry for 24 h before adding the bacteria. An overnight culture of *E. coli* OP50 was inoculated 1:100 and grown at 37°C to OD600nm=0.5-0.6. The bacteria were concentrated to OD600nm=4 before seeding onto plates with tunicamycin. Plates were dried at room temperature for 1 day before use. Embryos were obtained by standard bleaching of gravid adult and ~150 embryos were placed on each of 3 plates. Counting of L4 and adults was performed 72 h later. To examine tunicamycin sensitivity of worms treated with RNAi, embryos were transferred to RNAi feeding plates seeded with dsRNA-producing bacteria of the tested autophagy genes or with bacteria containing the empty feeding vector L4440 as a control as described in [74]. At least three independent experiments were performed for each tunicamycin concentration, RNAi clone or mutant. Statistical significance was determined by two-sample t-test after first testing for equal variance by F-test or by one-way ANOVA followed by Tukey's multiple comparisons test.

L1 survival assay

Gravid adults were bleached and ~10,000 embryos/ml were incubated in M9 buffer (86 mM NaCl, 22 mM KH_2PO4, 42 mM Na_2HPO_4, pH 7) in 15ml conical tubes, in a rotator at 20˚C for the indicated time points (starvation time). Day 1 of starvation counted as 24 h after bleaching. At each time point, a 20-µl aliquot (100-150 worms) was dropped on three NGM plates seeded with HB101, and placed at 20˚C.

After 3 days of recovery on food plates, worms that reached L4/adult were counted and averaged. The number of worms developed from day 1 of starvation (first time point) was used as control to calculate the number of dead worms at each time point. To apply log-rank statistics, survival rates were smoothed to a non-increasing function. The experimental noise (variability) was reduced by applying centered moving averaging over each consecutive three time points before the survival rate decreased to 90%. Therefore, the smoothing was performed only on the early time points of the survival curves, before significant numbers of animals had lost viability. The experimental noise is assumed to result from pipetting and counting errors. This correction allowed using OASIS - Online Application for Survival Analysis [75] for performing the Log-Rank statistics. The L1 survival assay showed some variability between experiments [11], therefore we compared populations assayed simultaneously (Table S1). The L1 survival shown in Fig. 2 is representative of 4 independent experiments (Table S1).

Lifespan assay of adults

Gravid adults were allowed to lay eggs on NGM plates seeded with OP50 for 3 h. Plates were maintained at 15˚C until larvae reached the 1st day of adulthood. 120 1st day adults were placed on NGM plates with 1 µM FUdR (Sigma, F0503) [76] at 20°C and this was determined as day 1 of lifespan counting (8 plates per strain). Animals were transferred to fresh NGM+FUdR plates every 48 h during the reproductive period, and if plates were contaminated thereafter. Animals were scored as dead when they failed to respond to touch. Animals that died from internal hatching, dried, exploded, disappeared, and worms on contamination were censored and removed from the plates. Statistical analysis of lifespan assays was calculated with Log-Rank test using OASIS- Online Application for Survival Analysis [75]. The lifespan data shown in Fig. 3 are representative of 3 independent experiments (Table S2).

Analysis of DAF-28::GFP reporter

3-day old transgenic animals were anaesthetized on 2% agarose pads containing 2 mM levamisole (Sigma, L9756). Images were taken with a CCD digital camera using a Nikon 90i fluorescence microscope. For each trial, exposure time was calibrated to minimize the number of saturated pixels and was kept constant through the experiment. The NIS element software was used to quantify total fluorescence intensity in selected areas including the head region (the DAF-28::GFP expressing neurons, Fig. 4C), the posterior intestine (the DAF-28::GFP expressing intestinal cells, Fig. 4D) and the body cavity of the animal (the area between the producing cells of the rear intestine and the middle of the animal, not including ceolomocytes, Fig. 4E). Note that the natural autofluorescence from the intestine significantly

contributes to the whole body fluorescence measurements, and accounts for the signal detected in the control and *ire-1* mutants (Fig. 4E). In addition, each animal was qualitatively scored for the accumulation of fluorescent GFP in the posterior intestine (Fig. 4B).

Quantitative proteomics profiling

We performed metabolic labeling with ^{15}N stable isotope followed by quantitative mass spectrometry (MS) [77, 78]. For labeling *C. elegans* with ^{15}N, the NA22 *E. coli* strain was grown ON in Spectra 9 medium (15N, 98%, Cambridge Isotope Laboratories, CGM-3030-N-1), pelleted and concentrated 10x. Worm plates were prepared with nitrogen-free medium including (12 g agarose [Amersco, 0710], 3 g NaCl, 1 ml 5 mg/ml cholesterol, 1 ml 1 M $CaCl_2$, 1 ml 1 M $MgCl_2$ and 25 ml 1 M K_2HPO_4/KH_2PO_4, pH 6.0 per liter). Worms were grown on either ^{15}N -labeled or unlabeled NA22 bacteria till the plate was almost cleared from bacteria and containing F1 and F2 progeny – this was considered one passage. Worms were transferred to new plates and were fed either ^{15}N -labeled or unlabeled bacteria for a second passage. For the third and final passage, plates were prepared with 50x concentrated bacteria. Tunicamycin (1 µg/ml) was spread and allowed to dry one day before adding the bacteria. The SJ4005 strain [5] was used as a control for ER stress induction on the tunicamycin plates. For each experiment, the control group was grown on unlabeled bacteria, and the experimental group carrying the *rnf-5(tm794)* allele was grown on ^{15}N labeled bacteria. Worms were collected and washed once in M9, the supernatant was removed, the pellet was frozen in liquid nitrogen and then stored at -80°C. Worm pellets were lysed with 1 volume of lysis buffer (20 mM HEPES, pH 7.4, 10 mM KCl, 1.5 mM $MgCl_2$, 1 mM DTT, and 2x EDTA-free protease inhibitor cocktail [Roche, 05 892 791 001]) . Worms were lysed by sonication and spun at 1000 g for 10 min. Protein was determined using BCA Protein Assay (Pierce, 23227). Supernatants of the 15N-labeled and unlabeled worms from the 1000 g spin were combined at a 1:1 protein ratio and centrifuged at 100,000 g for 1 h. A portion (1.2 mg) of each sample was methanol-chloroform precipitated, the pellet air-dried and frozen at -80°C. Tandem mass spectrometry (MS/MS), data analysis and protein quantification was performed according to [79] at the Proteomics Shared Resource facility, Sanford Burnham Prebys Medical Discovery Institute. Cutoff for differentially expressed proteins was protein ratio of 1.5(or 0.66) and p-value of 0.05 and 0.1. The data set was analyzed using DAVID [80] and STRING [63]. We analyzed two biological replicates and three technical replicates for each strain.

Heat stress assay

In this assay we considered many of the important notes and recommendations summarized in [4]. Mid-L4 larvae from a mixed population grown in 20°C (without bleach) were singly plated to freshly seeded OP50 (50 µl; OD=0.54) NGM plates and grown at 20°C for 24 h. Day 1 adult animals were shifted to 37°C for 5 h 30 min heat shock followed by recovery at 20°C for 12 h. Animals were counted for live (including very sick but alive *ire-1(v33)* animals) or dead animals. Worms were scored by gentle touch with a platinum transfer pick. Five independent repeats were performed and 40-50 worms for each strain were analyzed on single plates in each experiment. We decided to plate the worms individually before the heat stress treatment since in our hands it seems that there is a population effect on resistance to heat shock. Statistical analysis was conducted by one-way ANOVA followed by Tukey's multiple comparisons test.

RNF-5 transcriptional reporter

The Exrnf-5p::mCherry transcriptional reporter incudes 6.4kb upstream of *rnf-121*, the first gene in the operon of *rnf-5* (CEOP3156) followed by the mCherry coding sequence and let-858 3'UTR.

Lysosome quantification with LysoTracker

Following hatching in M9, 30-50 L1 animals were dropped on 24 well plates containing OP50 with final concentration of 2 µM LysoTracker Red DND-99 (Invitrogen, L7528). Day 1 adult animals were imaged using confocal microscopy (Zeiss LSM 5 Exciter). The anterior intestine immediately posterior to the pharyngeal-intestinal valve was imaged in all animals. Three independent experiments were performed and 10-20 animals from each genotype were imaged in each experiment. The diameter of the detection pinhole was set to 1 Airy. Images were collected at a fixed pixel size of 0.54 µm selecting a region of interest of 820X282 pixels. Quantification of the number and size of lysosomes in the same z-focal plane was carried out using a custom made ImageJ macro in Fiji [81]. In brief, lysosomes were detected using the 'adaptive threshold' plugin and the size measured using 'analyze particles' with a size exclusion of 20 pixels. Statistical analysis was conducted by one-way ANOVA followed by Tukey's multiple comparisons test. GFP::LGG-1 animals were stained with 2 µM LysoTracker Red DND-99 as described above and images were acquired using confocal system (Zeiss LSM 5 Exciter). GFP was excited using a 488 nm argon laser and the fluorescence emission was collected using a band pass 505 – 530 nm filter. LysoTracker Red DND-99 was excited using a 543 nm HeNe laser and the emission was collected using a long pass 560 nm laser.

Magic Red assay to measure lysosomal activity

Magic Red (ImmunoChemistry Technologies, 6133) produces red fluorescence following proteolytic cleavage by cathepsin B in functional lysosomes. Magic Red stain was prepared in 260x DMSO stock according to the manufacturer's instructions and 4 µl stock was diluted x10 with M9. The diluted stock (15 µl) was added into wells of a 24-well-plate containing 1 ml NGM and a dried circle of OP50. The plate was dried in dark after addition of the Magic Red solution. L4 stage worms were transferred (50 worms/well) and grown overnight at 20°C. Day 1 adult worms were washed with M9 and imaged with Nikon SMZ18 and the anterior intestine region was quantified by Fiji. Four independent experiments were performed with n ≥ 40. Statistical analysis was conducted by one-way ANOVA followed by Tukey's multiple comparisons test.

Statistical analysis

The data were presented as the mean ± SEM from at least 3 independent experiments. Statistical differences were determined as described above for each assay.

Acknowledgment

We thank WormBase for *C. elegans* genetic annotation. Several strains were provided by the Caenorhabditis Genetics Center (CGC), which is funded by NIH Office of Research Infrastructure Programs (P40 OD010440) and Dr. Shohei Mitani, National Bioresource Project for the nematode, Tokyo Women's Medical University School of Medicine, Japan. We thank Prof. Dieter A. Wolf from the Sanford Burnham Prebys Medical Discovery Institute for advices on proteomics analysis and comments on the manuscript. We thank Prof. Peter Naredi (Umea University, Sweden) for the DAF-28::GFP expressing strain. We thank Sharon Sheffy-Levin for sample preparation for the proteomics analysis and initial hit analysis and Hanna Grobe for writing and optimizing the ImageJ Macro for lysosome analysis.

Disclosure statement

No potential conflict of interest was reported by the authors.

Additional information

Funding

This research was supported by the Israel Science Foundation (ISF 1878/15 and 2122/19) and the Israel Cancer Research Fund PG-14-101 (to L.B.), and by the Ministry of Science, Technology & Space, Israel (3-12066) (to S.H-K).

References

1. Schröder M, Kaufman RJ: **THE MAMMALIAN UNFOLDED PROTEIN RESPONSE**. *Annual Review of Biochemistry* 2005, **74**:739-789.
2. Ron D, Walter P: **Signal integration in the endoplasmic reticulum unfolded protein response**. *Nature Reviews Molecular Cell Biology* 2007, **8**:519.
3. Vembar SS, Brodsky JL: **One step at a time: endoplasmic reticulum-associated degradation**. *Nature Reviews Molecular Cell Biology* 2008, **9**:944.
4. Hetz C: **The unfolded protein response: controlling cell fate decisions under ER stress and beyond**. *Nature Reviews Molecular Cell Biology* 2012, **13**:89-102.
5. Calfon M, Zeng H, Urano F, Till JH, Hubbard SR, Harding HP, Clark SG, Ron D: **IRE1 couples endoplasmic reticulum load to secretory capacity by processing the XBP-1 mRNA**. *Nature* 2002, **415**:92.
6. Gardner BM, Walter P: **Unfolded Proteins Are Ire1-Activating Ligands That Directly Induce the Unfolded Protein Response**. *Science* 2011, **333**:1891-1894.
7. Shen X, Ellis RE, Sakaki K, Kaufman RJ: **Genetic Interactions Due to Constitutive and Inducible Gene Regulation Mediated by the Unfolded Protein Response in C. elegans**. *PLOS Genetics* 2005, **1**:e37.
8. Richardson CE, Kinkel S, Kim DH: **Physiological IRE-1-XBP-1 and PEK-1 Signaling in Caenorhabditis elegans Larval Development and Immunity**. *PLOS Genetics* 2011, **7**:e1002391.
9. Safra M, Ben-Hamo S, Kenyon C, Henis-Korenblit S: **The ire-1 ER stress-response pathway is required for normal secretory-protein metabolism in C. elegans**. *Journal of Cell Science* 2013, **126**:4136-4146.
10. Henis-Korenblit S, Zhang P, Hansen M, McCormick M, Lee S-J, Cary M, Kenyon C: **Insulin/IGF-1 signaling mutants reprogram ER stress response regulators to promote longevity**. *Proceedings of the National Academy of Sciences* 2010, **107**:9730-9735.
11. Roux AE, Langhans K, Huynh W, Kenyon C: **Reversible Age-Related Phenotypes Induced during Larval Quiescence in C. elegans**. *Cell Metabolism* 2016, **23**:1113-1126.
12. Ohsumi Y: **Historical landmarks of autophagy research**. *Cell Research* 2013, **24**:9.
13. Levine B, Klionsky DJ: **Development by Self-Digestion: Molecular Mechanisms and Biological Functions of Autophagy**. *Dev Cell* 2004, **6**:463-477.
14. Nakatogawa H, Suzuki K, Kamada Y, Ohsumi Y: **Dynamics and diversity in autophagy mechanisms: lessons from yeast**. *Nature Reviews Molecular Cell Biology* 2009, **10**:458-467.
15. Feng Y, He D, Yao Z, Klionsky DJ: **The machinery of macroautophagy**. *Cell Research* 2014, **24**:24-41.
16. Palmisano NJ, Meléndez A: **Autophagy in C. elegans development**. *Developmental Biology* 2019, **447**:103-125.
17. Mizushima N, Komatsu M: **Autophagy: Renovation of Cells and Tissues**. *Cell* 2011, **147**:728-741.
18. Kroemer G, Mariño G, Levine B: **Autophagy and the Integrated Stress Response**. *Molecular Cell* 2010, **40**:280-293.
19. Kaur J, Debnath J: **Autophagy at the crossroads of catabolism and anabolism**. *Nature Reviews Molecular Cell Biology* 2015, **16**:461-472.
20. Bachar-Wikstrom E, Wikstrom JD, Kaiser N, Cerasi E, Leibowitz G: **Improvement of ER stress-induced diabetes by stimulating autophagy**. *Autophagy* 2013, **9**:626-628.

21. Ogata M, Hino S-i, Saito A, Morikawa K, Kondo S, Kanemoto S, Murakami T, Taniguchi M, Tanii I, Yoshinaga K, et al.: **Autophagy Is Activated for Cell Survival after Endoplasmic Reticulum Stress**. *Molecular and Cellular Biology* 2006, **26**:9220-9231.
22. Rzymski T, Milani M, Pike L, Buffa F, Mellor HR, Winchester L, Pires I, Hammond E, Ragoussis I, Harris AL: **Regulation of autophagy by ATF4 in response to severe hypoxia**. *Oncogene* 2010, **29**:4424-4435.
23. Song S, Tan J, Miao Y, Zhang Q: **Crosstalk of ER stress-mediated autophagy and ER-phagy: Involvement of UPR and the core autophagy machinery**. *Journal of Cellular Physiology* 2018, **233**:3867-3874.
24. Yorimitsu T, Nair U, Yang Z, Klionsky DJ: **Endoplasmic Reticulum Stress Triggers Autophagy**. *Journal of Biological Chemistry* 2006, **281**:30299-30304.
25. Bernales S, McDonald KL, Walter P: **Autophagy Counterbalances Endoplasmic Reticulum Expansion during the Unfolded Protein Response**. *PLOS Biology* 2006, **4**:e423.
26. Kouroku Y, Fujita E, Tanida I, Ueno T, Isoai A, Kumagai H, Ogawa S, Kaufman RJ, Kominami E, Momoi T: **ER stress (PERK/eIF2α phosphorylation) mediates the polyglutamine-induced LC3 conversion, an essential step for autophagy formation**. *Cell Death & Differentiation* 2007, **14**:230-239.
27. Senft D, Ronai ZeA: **UPR, autophagy, and mitochondria crosstalk underlies the ER stress response**. *Trends in Biochemical Sciences* 2015, **40**:141-148.
28. Muscarella DE, Bloom SE: **The contribution of c-Jun N-terminal kinase activation and subsequent Bcl-2 phosphorylation to apoptosis induction in human B-cells is dependent on the mode of action of specific stresses**. *Toxicology and Applied Pharmacology* 2008, **228**:93-104.
29. Yamamoto K, Ichijo H, Korsmeyer SJ: **BCL-2 Is Phosphorylated and Inactivated by an ASK1/Jun N-Terminal Protein Kinase Pathway Normally Activated at G₂/M**. *Molecular and Cellular Biology* 1999, **19**:8469-8478.
30. Zalckvar E, Berissi H, Mizrachy L, Idelchuk Y, Koren I, Eisenstein M, Sabanay H, Pinkas-Kramarski R, Kimchi A: **DAP-kinase-mediated phosphorylation on the BH3 domain of beclin 1 promotes dissociation of beclin 1 from Bcl-XL and induction of autophagy**. *EMBO reports* 2009, **10**:285-292.
31. Pattingre S, Tassa A, Qu X, Garuti R, Liang XH, Mizushima N, Packer M, Schneider MD, Levine B: **Bcl-2 Antiapoptotic Proteins Inhibit Beclin 1-Dependent Autophagy**. *Cell* 2005, **122**:927-939.
32. Pattingre S, Bauvy C, Carpentier S, Levade T, Levine B, Codogno P: **Role of JNK1-dependent Bcl-2 Phosphorylation in Ceramide-induced Macroautophagy**. *Journal of Biological Chemistry* 2009, **284**:2719-2728.
33. Margariti A, Li H, Chen T, Martin D, Vizcay-Barrena G, Alam S, Karamariti E, Xiao Q, Zampetaki A, Zhang Z, et al.: **XBP1 mRNA Splicing Triggers an Autophagic Response in Endothelial Cells through BECLIN-1 Transcriptional Activation**. *Journal of Biological Chemistry* 2013, **288**:859-872.
34. Imanikia S, Özbey NP, Krueger C, Casanueva MO, Taylor RC: **Neuronal XBP-1 Activates Intestinal Lysosomes to Improve Proteostasis in C. elegans**. *Current Biology* 2019, **29**:2322-2338.e2327.
35. B'chir W, Maurin A-C, Carraro V, Averous J, Jousse C, Muranishi Y, Parry L, Stepien G, Fafournoux P, Bruhat A: **The eIF2α/ATF4 pathway is essential for stress-induced autophagy gene expression**. *Nucleic Acids Research* 2013, **41**:7683-7699.
36. Høyer-Hansen M, Bastholm L, Szyniarowski P, Campanella M, Szabadkai G, Farkas T, Bianchi K, Fehrenbacher N, Elling F, Rizzuto R, et al.: **Control of Macroautophagy by Calcium, Calmodulin-Dependent Kinase Kinase-β, and Bcl-2**. *Molecular Cell* 2007, **25**:193-205.
37. Younger JM, Chen L, Ren H-Y, Rosser MFN, Turnbull EL, Fan C-Y, Patterson C, Cyr DM: **Sequential Quality-Control Checkpoints Triage Misfolded Cystic Fibrosis Transmembrane Conductance Regulator**. *Cell* 2006, **126**:571-582.

38. Delaunay A, Bromberg KD, Hayashi Y, Mirabella M, Burch D, Kirkwood B, Serra C, Malicdan MC, Mizisin AP, Morosetti R, et al.: **The ER-Bound RING Finger Protein 5 (RNF5/RMA1) Causes Degenerative Myopathy in Transgenic Mice and Is Deregulated in Inclusion Body Myositis**. *PLoS ONE* 2008, **3**:e1609.
39. Kuang E, Qi J, Ronai Ze: **Emerging roles of E3 ubiquitin ligases in autophagy**. *Trends in Biochemical Sciences* 2013, **38**:453-460.
40. Tomati V, Sondo E, Armirotti A, Caci E, Pesce E, Marini M, Gianotti A, Ju Jeon Y, Cilli M, Pistorio A, et al.: **Genetic Inhibition Of The Ubiquitin Ligase Rnf5 Attenuates Phenotypes Associated To F508del Cystic Fibrosis Mutation**. *Scientific Reports* 2015, **5**:12138.
41. Sondo E, Falchi F, Caci E, Ferrera L, Giacomini E, Pesce E, Tomati V, Mandrup Bertozzi S, Goldoni L, Armirotti A, et al.: **Pharmacological Inhibition of the Ubiquitin Ligase RNF5 Rescues F508del-CFTR in Cystic Fibrosis Airway Epithelia**. *Cell Chemical Biology* 2018, **25**:891-905.e898.
42. Morito D, Hirao K, Oda Y, Hosokawa N, Tokunaga F, Cyr DM, Tanaka K, Iwai K, Nagata K: **Gp78 Cooperates with RMA1 in Endoplasmic Reticulum-associated Degradation of CFTRΔF508**. *Mol Biol Cell* 2008, **19**:1328-1336.
43. Jeon Young J, Khelifa S, Ratnikov B, Scott David A, Feng Y, Parisi F, Ruller C, Lau E, Kim H, Brill Laurence M, et al.: **Regulation of Glutamine Carrier Proteins by RNF5 Determines Breast Cancer Response to ER Stress-Inducing Chemotherapies**. *Cancer Cell* 2015, **27**:354-369.
44. Zhong B, Zhang L, Lei C, Li Y, Mao A-P, Yang Y, Wang Y-Y, Zhang X-L, Shu H-B: **The Ubiquitin Ligase RNF5 Regulates Antiviral Responses by Mediating Degradation of the Adaptor Protein MITA**. *Immunity* 2009, **30**:397-407.
45. Zhong B, Zhang Y, Tan B, Liu T-T, Wang Y-Y, Shu H-B: **The E3 Ubiquitin Ligase RNF5 Targets Virus-Induced Signaling Adaptor for Ubiquitination and Degradation**. *The Journal of Immunology* 2010, **184**:6249-6255.
46. Li Y, Tinoco R, Elmén L, Segota I, Xian Y, Fujita Y, Sahu A, Zarecki R, Marie K, Feng Y, et al.: **Gut microbiota dependent anti-tumor immunity restricts melanoma growth in Rnf5−/− mice**. *Nature communications* 2019, **10**:1492.
47. Kuang E, Okumura CYM, Sheffy-Levin S, Varsano T, Shu VC-W, Qi J, Niesman IR, Yang H-J, López-Otín C, Yang WY, et al.: **Regulation of ATG4B Stability by RNF5 Limits Basal Levels of Autophagy and Influences Susceptibility to Bacterial Infection**. *PLOS Genetics* 2012, **8**:e1003007.
48. Broday L, Kolotuev I, Didier C, Bhoumik A, Podbilewicz B, Ronai Ze: **The LIM domain protein UNC-95 is required for the assembly of muscle attachment structures and is regulated by the RING finger protein RNF-5 in C. elegans**. *The Journal of Cell Biology* 2004, **165**:857-867.
49. Zaidel-Bar R, Miller S, Kaminsky R, Broday L: **Molting-specific downregulation of C. elegans body-wall muscle attachment sites: The role of RNF-5 E3 ligase**. *Biochemical and Biophysical Research Communications* 2010, **395**:509-514.
50. Kovacevic I, Ho R, Cram EJ: **CCDC-55 is required for larval development and distal tip cell migration in C. elegans**. *Mechanisms of Development* 2012, **128**:548-559.
51. Didier C, Broday L, Bhoumik A, Israeli S, Takahashi S, Nakayama K, Thomas SM, Turner CE, Henderson S, Sabe H, et al.: **RNF5, a RING finger protein that regulates cell motility by targeting paxillin ubiquitination and altered localization**. *Mol Cell Biol* 2003, **23**:5331-5345.
52. Baugh LR: **To Grow or Not to Grow: Nutritional Control of Development During Caenorhabditis elegans L1 Arrest**. *Genetics* 2013, **194**:539-555.
53. Muñoz MJ, Riddle DL: **Positive selection of Caenorhabditis elegans mutants with increased stress resistance and longevity**. *Genetics* 2003, **163**:171-180.
54. Baugh LR, Sternberg PW: **DAF-16/FOXO Regulates Transcription of cki-1/Cip/Kip and Repression of lin-4 during C. elegans L1 Arrest**. *Current Biology* 2006, **16**:780-785.

55. Chang JT, Kumsta C, Hellman AB, Adams LM, Hansen M: **Spatiotemporal regulation of autophagy during Caenorhabditis elegans aging**. *eLife* 2017, **6**:e18459.
56. Tian Y, Li Z, Hu W, Ren H, Tian E, Zhao Y, Lu Q, Huang X, Yang P, Li X, et al.: **C. elegans Screen Identifies Autophagy Genes Specific to Multicellular Organisms**. *Cell* 2010, **141**:1042-1055.
57. Ichimura Y, Kirisako T, Takao T, Satomi Y, Shimonishi Y, Ishihara N, Mizushima N, Tanida I, Kominami E, Ohsumi M, et al.: **A ubiquitin-like system mediates protein lipidation**. *Nature* 2000, **408**:488-492.
58. Zhang Y, Yan L, Zhou Z, Yang P, Tian E, Zhang K, Zhao Y, Li Z, Song B, Han J, et al.: **SEPA-1 Mediates the Specific Recognition and Degradation of P Granule Components by Autophagy in C. elegans**. *Cell* 2009, **136**:308-321.
59. Kang C, You Y-j, Avery L: **Dual roles of autophagy in the survival of Caenorhabditis elegans during starvation**. *Genes & Development* 2007, **21**:2161-2171.
60. Kao G, Nordenson C, Still M, Rönnlund A, Tuck S, Naredi P: **ASNA-1 Positively Regulates Insulin Secretion in C. elegans and Mammalian Cells**. *Cell* 2007, **128**:577-587.
61. Safra M, Henis-Korenblit S: **A new tool in C. elegans reveals changes in secretory protein metabolism in ire-1-deficient animals**. *Worm* 2014, **3**:e27733.
62. Safra M, Fickentscher R, Levi-Ferber M, Danino Yehuda M, Haviv-Chesner A, Hansen M, Juven-Gershon T, Weiss M, Henis-Korenblit S: **The FOXO Transcription Factor DAF-16 Bypasses ire-1 Requirement to Promote Endoplasmic Reticulum Homeostasis**. *Cell Metabolism* 2014, **20**:870-881.
63. Szklarczyk D, Morris JH, Cook H, Kuhn M, Wyder S, Simonovic M, Santos A, Doncheva NT, Roth A, Bork P, et al.: **The STRING database in 2017: quality-controlled protein–protein association networks, made broadly accessible**. *Nucleic Acids Research* 2017, **45**:D362-D368.
64. Levine B, Kroemer G: **Biological Functions of Autophagy Genes: A Disease Perspective**. *Cell* 2019, **176**:11-42.
65. Thorburn A: **Autophagy and Its Effects: Making Sense of Double-Edged Swords**. *PLOS Biology* 2014, **12**:e1001967.
66. Levi-Ferber M, Salzberg Y, Safra M, Haviv-Chesner A, Bülow HE, Henis-Korenblit S: **It's All in Your Mind: Determining Germ Cell Fate by Neuronal IRE-1 in C. elegans**. *PLOS Genetics* 2014, **10**:e1004747.
67. Bohnert KA, Kenyon C: **A lysosomal switch triggers proteostasis renewal in the immortal C. elegans germ lineage**. *Nature* 2017, **551**:629-633.
68. Hughes AL, Gottschling DE: **An early age increase in vacuolar pH limits mitochondrial function and lifespan in yeast**. *Nature* 2012, **492**:261-265.
69. Gruidl ME, Smith PA, Kuznicki KA, McCrone JS, Kirchner J, Roussell DL, Strome S, Bennett KL: **Multiple potential germ-line helicases are components of the germ-line-specific P granules of Caenorhabditis elegans**. *Proceedings of the National Academy of Sciences of the United States of America* 1996, **93**:13837-13842.
70. Takeuchi O, Akira S: **Pattern Recognition Receptors and Inflammation**. *Cell* 2010, **140**:805-820.
71. Yunger E, Safra M, Levi-Ferber M, Haviv-Chesner A, Henis-Korenblit S: **Innate immunity mediated longevity and longevity induced by germ cell removal converge on the C-type lectin domain protein IRG-7**. *PLOS Genetics* 2017, **13**:e1006577.
72. Zou Z, Yuan Z, Zhang Q, Long Z, Chen J, Tang Z, Zhu Y, Chen S, Xu J, Yan M, et al.: **Aurora kinase A inhibition-induced autophagy triggers drug resistance in breast cancer cells**. *Autophagy* 2012, **8**:1798-1810.
73. Broday L, Kolotuev I, Didier C, Bhoumik A, Podbilewicz B, Ronai Z: **The LIM domain protein UNC-95 is required for the assembly of muscle attachment structures and is regulated by the RING finger protein RNF-5 in C. elegans**. *J Cell Biol* 2004, **165**:857-867.

74. Tsur A, Bening Abu-Shach U, Broday L: **ULP-2 SUMO Protease Regulates E-Cadherin Recruitment to Adherens Junctions**. *Dev Cell* 2015, **35**:63-77.
75. Yang J-S, Nam H-J, Seo M, Han SK, Choi Y, Nam HG, Lee S-J, Kim S: **OASIS: Online Application for the Survival Analysis of Lifespan Assays Performed in Aging Research**. *PLoS ONE* 2011, **6**:e23525.
76. Mitchell DH, Stiles JW, Santelli J, Sanadi DR: **Synchronous growth and aging of Caenorhabditis elegans in the presence of fluorodeoxyuridine**. *J Gerontol* 1979, **34**:28-36.
77. Krijgsveld J, Ketting RF, Mahmoudi T, Johansen J, Artal-Sanz M, Verrijzer CP, Plasterk RHA, Heck AJR: **Metabolic labeling of C. elegans and D. melanogaster for quantitative proteomics**. *Nature Biotechnology* 2003, **21**:927.
78. Dong M-Q, Venable JD, Au N, Xu T, Park SK, Cociorva D, Johnson JR, Dillin A, Yates JR: **Quantitative Mass Spectrometry Identifies Insulin Signaling Targets in C. elegans**. *Science* 2007, **317**:660-663.
79. Wu S, Zhu W, Nhan T, Toth JI, Petroski MD, Wolf DA: **CAND1 controls in vivo dynamics of the Cullin 1-RING ubiquitin ligase repertoire**. *Nature communications* 2013, **4**:1642-1642.
80. Huang DW, Sherman BT, Lempicki RA: **Systematic and integrative analysis of large gene lists using DAVID bioinformatics resources**. *Nature Protocols* 2008, **4**:44.
81. Schindelin J, Arganda-Carreras I, Frise E, Kaynig V, Longair M, Pietzsch T, Preibisch S, Rueden C, Saalfeld S, Schmid B, et al.: **Fiji: an open-source platform for biological-image analysis**. *Nature Methods* 2012, **9**:676-682.
82. Szklarczyk D, Gable AL, Lyon D, Junge A, Wyder S, Huerta-Cepas J, Simonovic M, Doncheva NT, Morris JH, Bork P, et al.: **STRING v11: protein–protein association networks with increased coverage, supporting functional discovery in genome-wide experimental datasets**. *Nucleic Acids Research* 2018, **47**:D607-D613.

Figure Legends

Figure 1. Inactivation of RNF-5 increases resistance to tunicamycin when autophagy is intact and partially rescues *ire-1* mutant animals. (**A**) N2 (wild-type) and *rnf-5(tm794)* embryos were treated with the indicated concentrations of tunicamycin. L4 larvae and adult animals were counted after 72 h incubation at 20°C. The mean values and SEM are shown. p<0.001(**), and p<0.0001 (***) by t-test. (**B**) N2 and *rnf-5(tm794)* embryos were treated with 1.5 µg/ml tunicamycin on RNAi plates of the autophagy genes indicated. The mean values and SEM are shown. Statistical significance was calculated by one-way ANOVA F(13,76)=22.19, P value < 0.0001, followed by Tukey's multiple comparisons test p<0.02 (*), p<0.0005(**), and p<0.0001 (***). (**C**) Double mutant *rnf-5;ire-1* improves development under physiological conditions and ER stress when compared to single *ire-1* mutant. *N* is the total number of plates analyzed (~150 embryos/plate) in 3-5 experiments. The mean values and SEM are shown. Statistical significance was calculated by one-way ANOVA F(7,157)=22.79, P value < 0.0001, followed by Tukey's multiple comparisons test p<0.03 (*), p<0.007(**), and p<0.0001 (***).

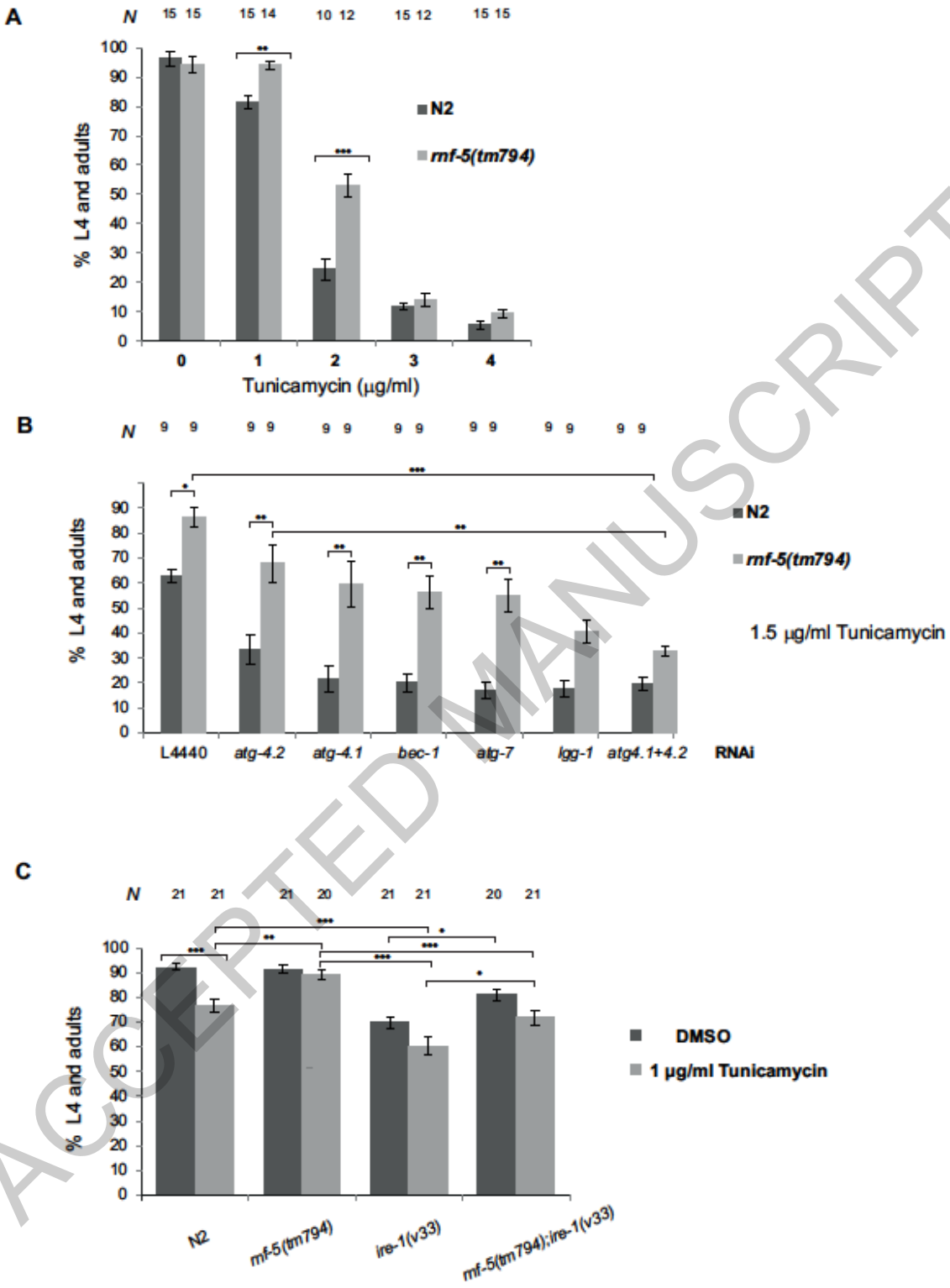

Figure 2. Increased survival of L1 arrest in double mutant *ire-1;rnf-5* compared to *ire-1* single mutant. (**A**) Survival rates of *rnf-5;ire-1* double mutant are higher than *ire-1* single mutant. (**B**) Survival rates of *atg-3* single mutant and *atg-3;rnf-5* double mutant are lower than wild-type and *rnf-5* single mutant. (**C**) Survival rates of *atg-3;ire-1* double mutant are lower than single *atg-3* or *ire-1* mutants. (**D**) Survival rates of *atg-3(bp412);rnf-5(tm794);ire-1(v33)* triple mutant are lower than *rnf-5(tm794);ire-1(v33)* double mutant. Animals were incubated in M9 buffer without food for the indicated time points and then dropped on plates with OP50 bacteria (food). The percentage of worms developed into L4 larvae and adults during 3 days of re-feeding is shown. Errors bars are the SEs at each time point indicated. (**E**) DIC images at day 10 of L1 arrest. Arrows point to dying cells.

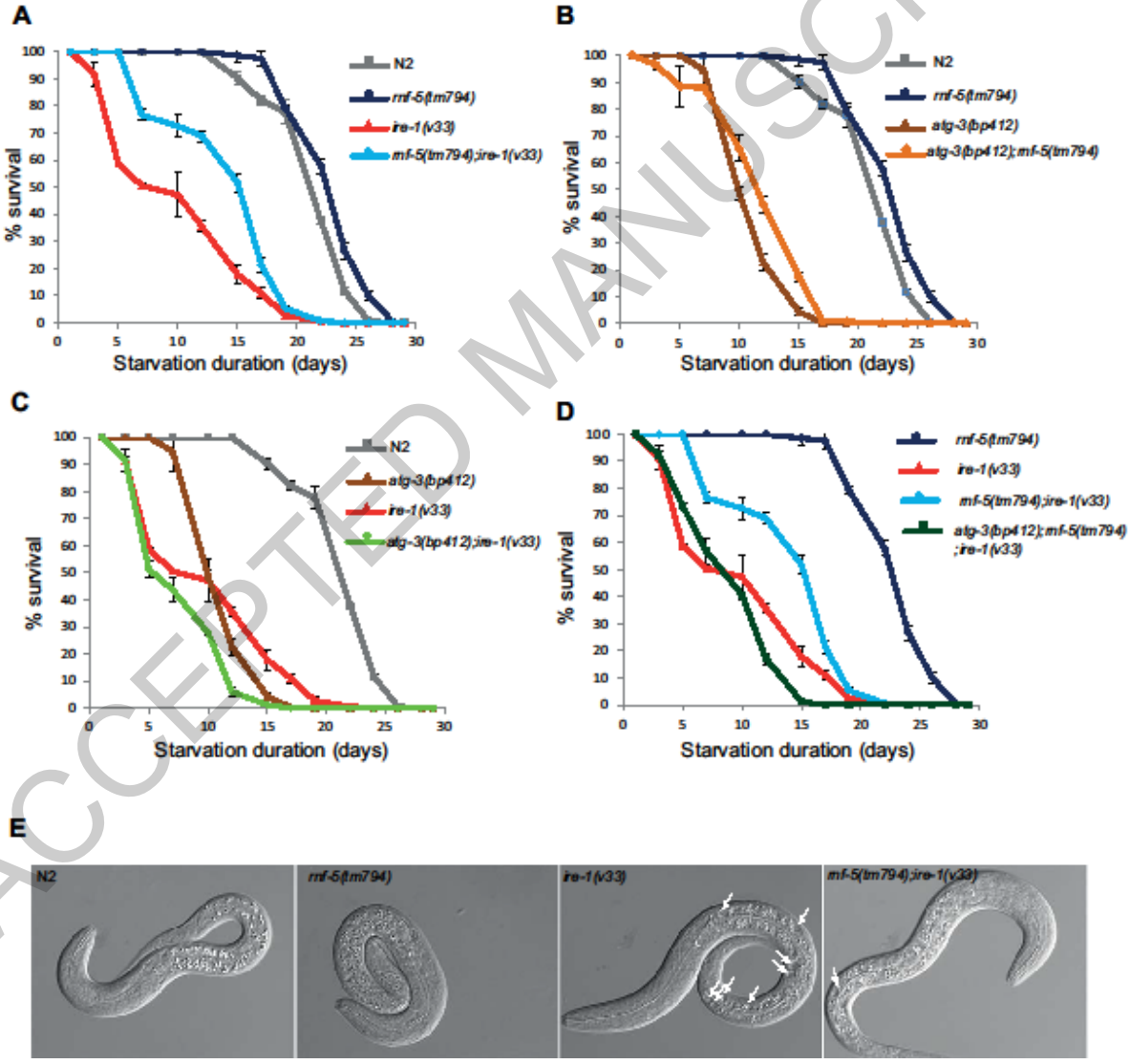

Figure 3. Extended lifespan of double mutant *ire-1;rnf-5* compared to *ire-1* single mutant. (**A**) Lifespan extension of *rnf-5;ire-1* double mutant compared to *ire-1* single mutant. (**B**) Lifespan of *atg-3* single mutant and *atg-3;rnf-5* double mutant is shorter compared to wild-type and *rnf-5* single mutant. (**C**) Lifespan of *atg-3;ire-1* double mutant is shorter than single *atg-3* or *ire-1* mutants. (**D**) Lifespan of *atg-3(bp412);rnf-5(tm794);ire-1(v33)* triple mutant are shorter than *rnf-5(tm794);ire-1(v33)* double mutant.

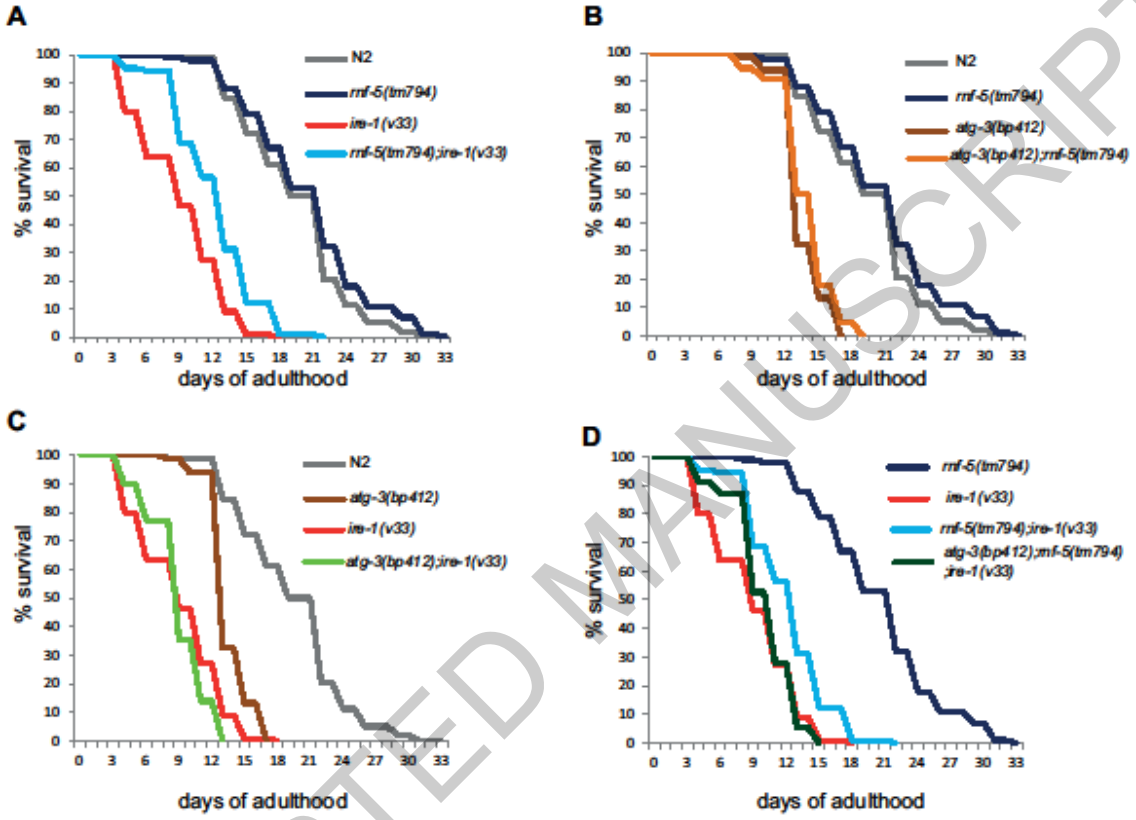

Figure 4. RNF-5 inactivation restores DAF-28::GFP secretion from the intestine of *ire-1* mutants. (**A**) Representative fluorescence micrographs of day-3 transgenic animals of the indicated genotype expressing an integrated DAF-28::GFP transgene. Arrowheads indicate DAF-28::GFP in the coelomocytes (white arrows), in the posterior intestine (yellow arrows) and in the anterior sensory neurons (green arrows). (**B**) Percentage of transgenic animals of the indicated genetic backgrounds with high levels of DAF-28::GFP in their body cavity (each animal was qualitatively scored for the accumulation of fluorescent GFP in the posterior intestine). (**C-E**) Bar graphs showing the relative mean fluorescence measured in the DAF-28::GFP expressing neurons (C), in the DAF-28::GFP expressing intestinal cells (D) and in the body cavity of the animals (E). Note that the *rnf-5* mutation increases the GFP signal beyond background autofluorescence from the intestine (see materials and methods). More than 45 animals

were analyzed per strain. In C and D, values are the normalized total fluorescence ± SEM. In E, values are the normalized mean fluorescence ± SEM $p<0.05$ (*), $p<0.001$(**), and $p<0.0001$ (***) by t-test.

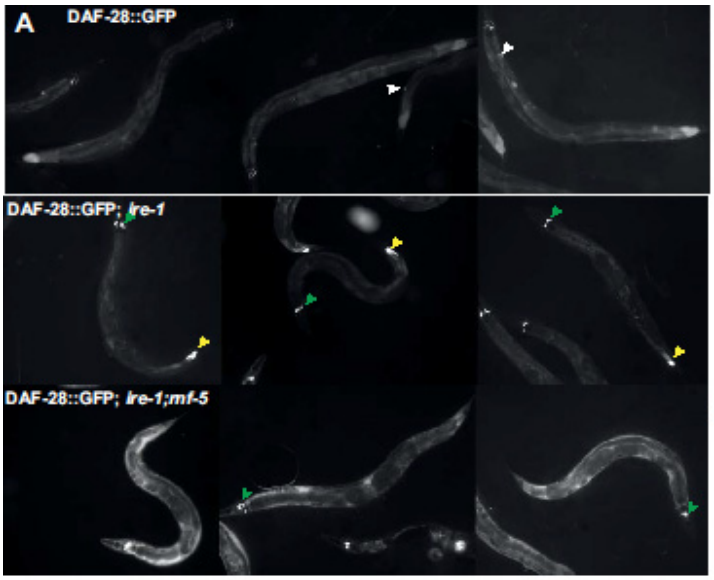

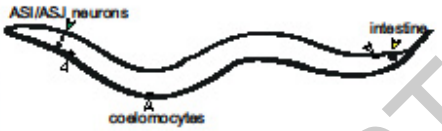

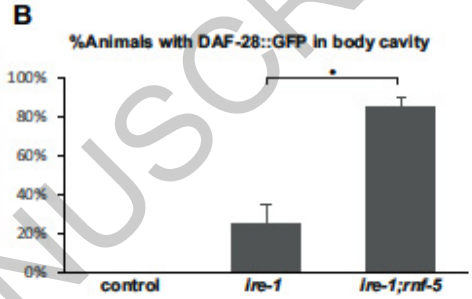

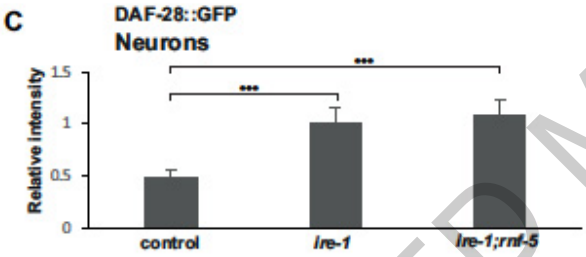

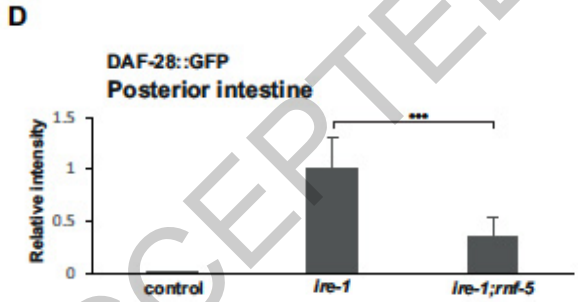

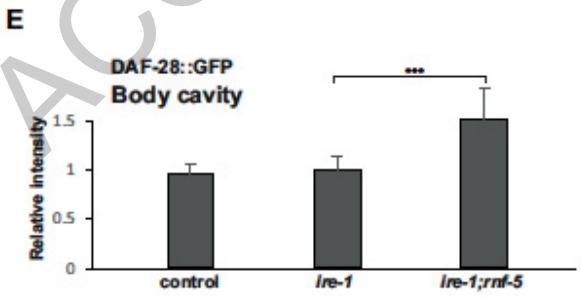

Figure 5. Increased levels of lysosomal proteases and RNA helicases in *rnf-5(tm794)* mutant animals. (**A**) Protein-protein interactions for differentially expressed proteins identified in a proteomics screen of *rnf-5(tm794)* and wild type animals grown on 1 µg/ml Tunicamycin (mild ER stress). Analysis was performed with STRING software (string-db.org) [82]. The network plot is based on known and predicted interactions (enrichment p-value: 1.9e-12). Two main clusters were identified: lysosomal proteases (marked red, clustering coefficient 0.832) and RNA helicases (marked purple, clustering coefficient 0.667). AIR-1 (labeled with asterisk) was downregulated in *rnf-5(tm794)* mutant worms compared to wild type. The entire list of differentially expressed proteins is presented in Table S3. (**B**) Representative fluorescence micrographs of day-1 adult GFP::LGG-1 and *rnf-5(tm794)*;GFP::LGG-1 stained with LysoTracker Red DND-99. The region of the anterior intestine is shown, n>20. Scale bar: 10 µm. (**C**) Representative fluorescence micrographs of day-1 adult wild type, *rnf-5(tm794)*, *ire-1(v33)* and *rnf-5(tm794);ire-1(v33)* animals stained with LysoTracker Red DND-99. Scale bar: 10 µm. (**D**) Intestinal lysosome quantification using LysoTracker Red DND-99 staining. The graphs show the number of lysosomes and the average lysosome size in each animal (1µm = 10.7 pixels). The mean values and SEM are shown in black. n=25 animals were imaged and analyzed for each genotype in 3 independent experiments. Statistical significance was calculated by one-way ANOVA $F(3,97)=52.63$ for the analysis of the number of lysosomes, $F(3,96)=12.66$ for the analysis of lysosome size, P value < 0.0001, followed by Tukey's multiple comparisons test $p<0.002$ (*), $p<0.0004$(**), and $p<0.0001$ (***).

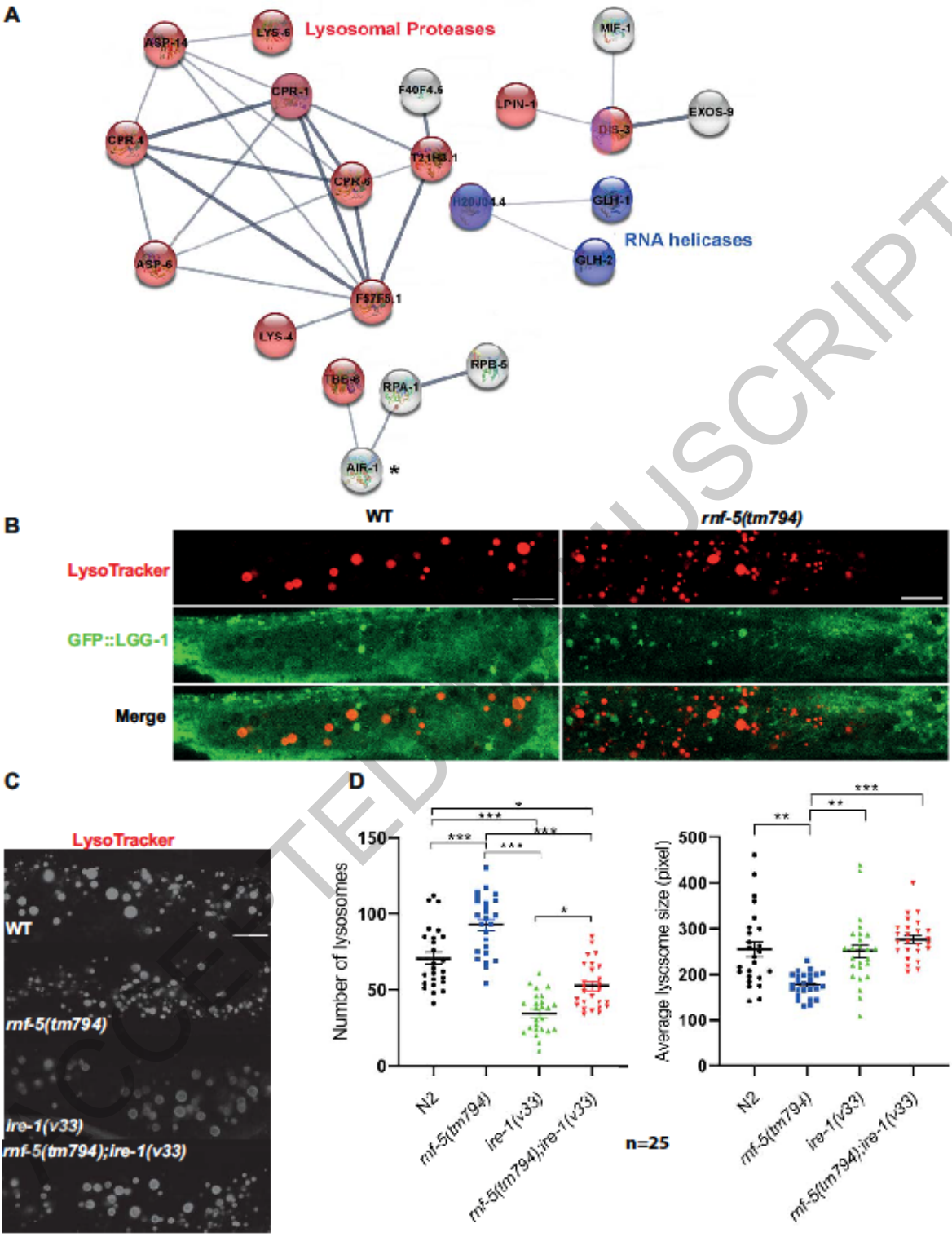

Supplementary Figures Adir et al.

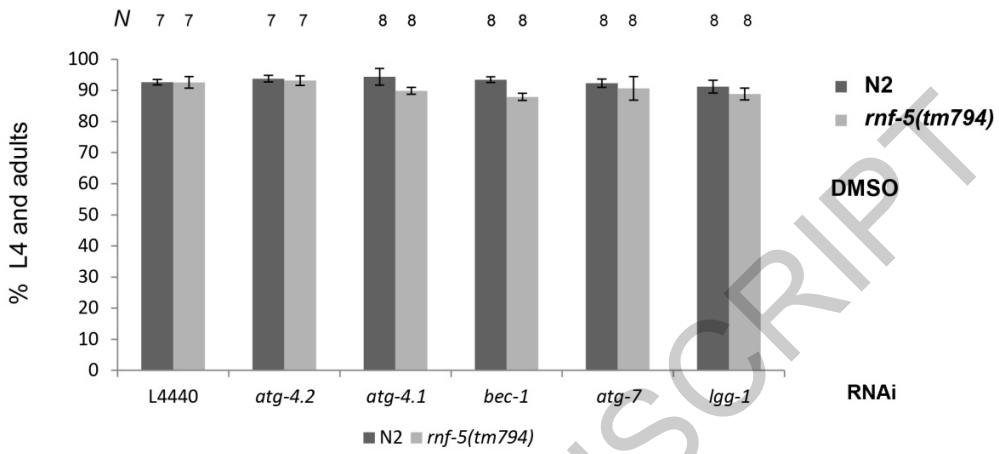

Figure S1. DMSO control for Figure 1B. N2 and *rnf-5(tm794)* embryos were treated with DMSO (same amount that was used in Figure 1B to dissolve tunicamaycin to 1.5 µg/ml) on RNAi plates of the autophagy genes indicated. L4 larvae and adult animals were counted after 72-h incubation at 20°C. The differences in the numbers of L4 and adults between the L4440 (control) and each of the RNAi treatments of the autophagy genes in both N2 and *rnf-5(tm794)* were all non-significant (by one-way ANOVA). *N* is the total number of plates analyzed (~150 embryos/plate) in 3 experiments.

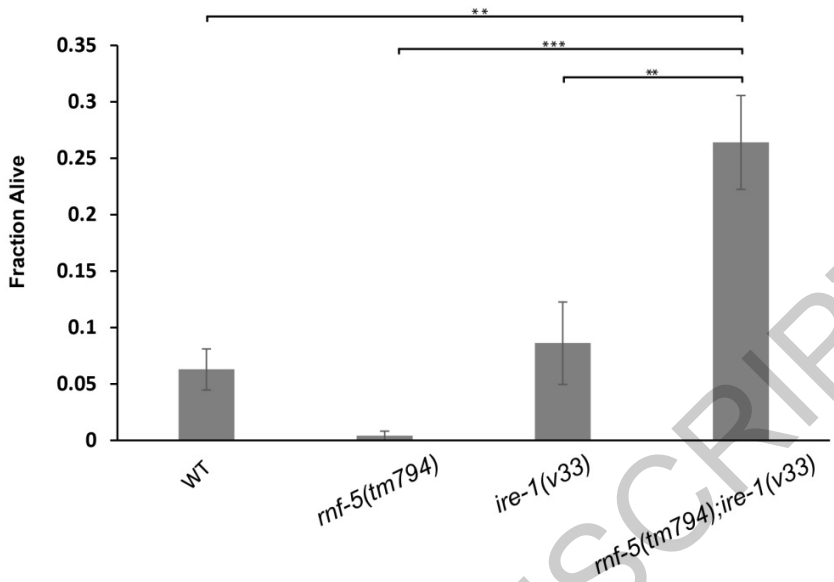

Figure S2. Double-mutant *rnf-5;ire-1* confers increased resistance to heat stress. Day 1 adults were heat shocked in 37°C and scored for survival after recovery in 20°C. Bar graph shows the fraction of worms alive after treatment. Statistical significance was calculated by one-way ANOVA, $F(3,16)=14.69$, P value < 0.0001, followed by Tukey's multiple comparisons test $p<0.003$(**), and $p<0.0001$ (***).

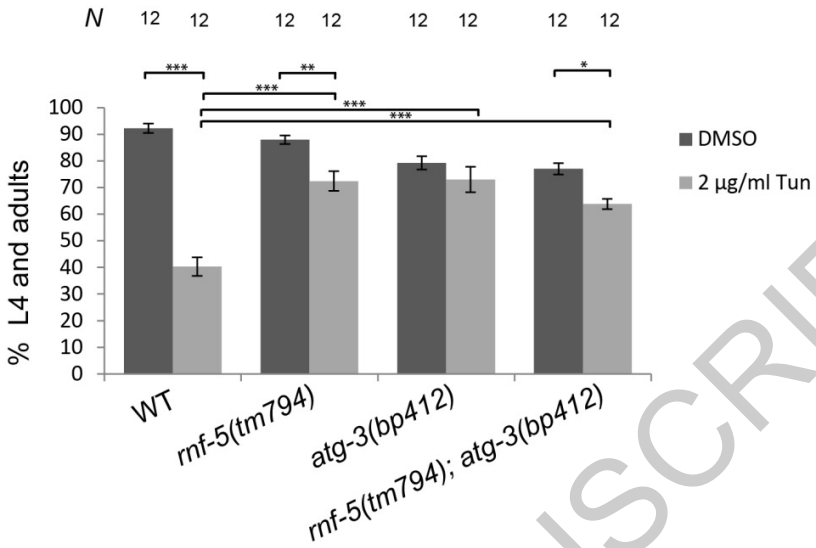

Figure S3. Inactivation of RNF-5 does not affect low sensitivity to tunicamycin in *atg-3(bp412)* mutant animals. N2, *rnf-5(tm794), atg-3(bp412)* and *rnf-5(tm794);atg-3(bp412)* embryos were treated with 2µg/ml tunicamycin. L4 larvae and adults animals were counted after a 72-h incubation at 20°C. *N* is the total number of plates analyzed (~150 embryos/plate) in 3 experiments. Statistical significance was calculated by one-way ANOVA $F(7,87)=28.54$, P value < 0.0001, followed by Tukey's multiple comparisons test $p<0.05$ (*), $p<0.007$(**), and $p<0.0001$ (***).

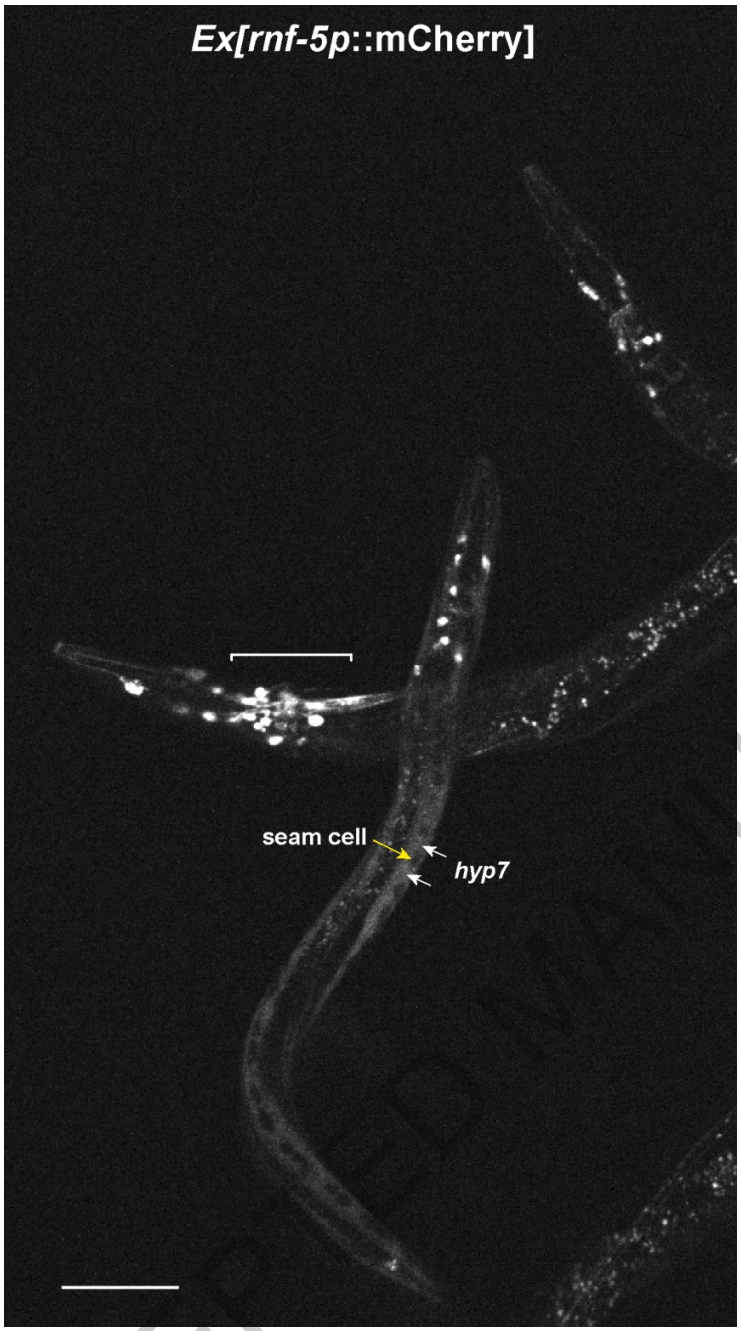

Figure S4. RNF-5 is expressed in head and tail neurons and the epidermis. The *rnf-5p*::mCherry reporter is expressed in head and tail neurons and in the epidermis (hyp7, white arrows). No expression is detected in the seam cells (yellow arrow). Scale bar: 50 µm.

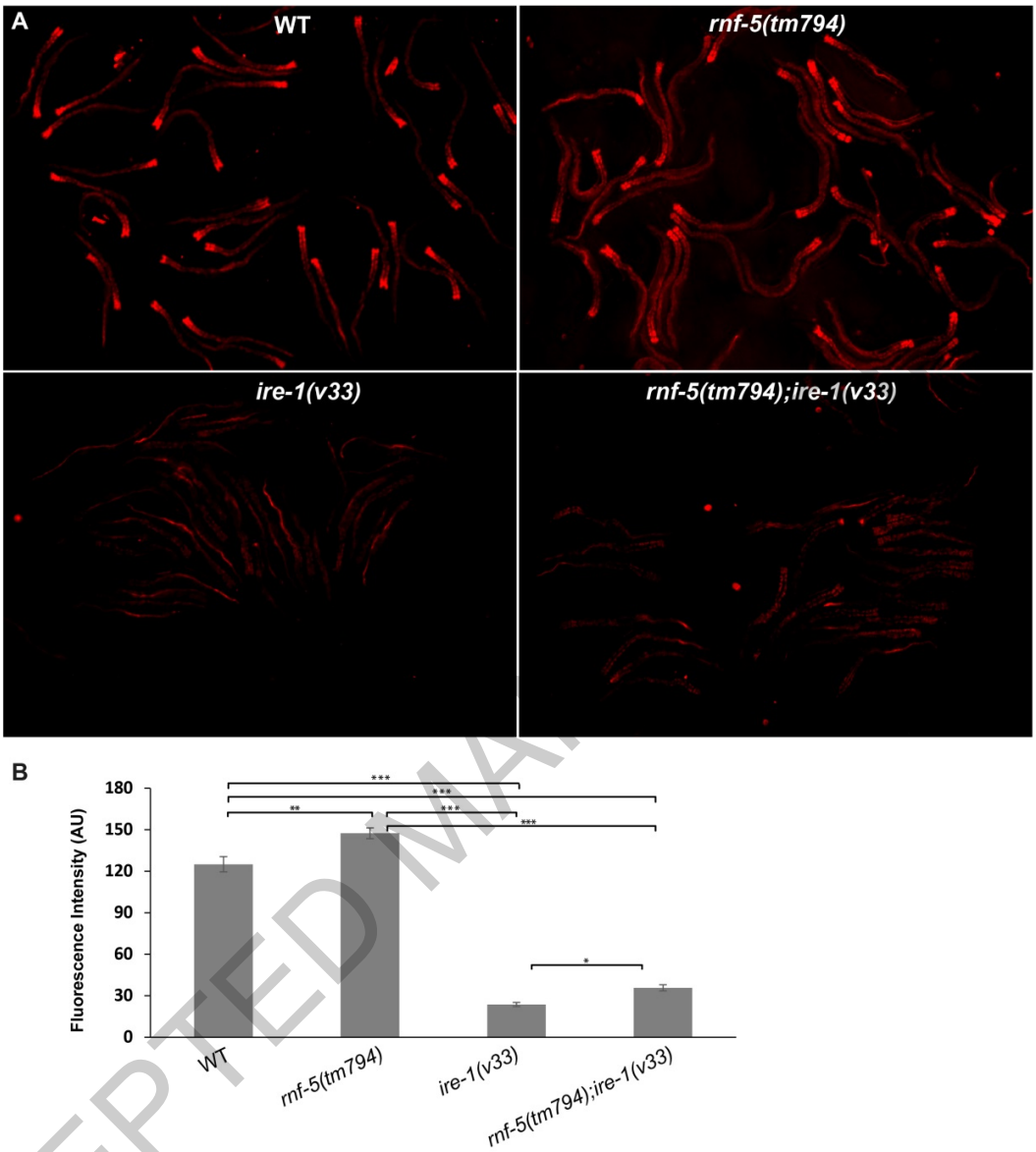

Figure S5. Inactivation of RNF-5 enhances lysosomal proteolytic activity. (A) Representative fluorescent images of day 1 adults stained with Magic Red fluorophore in wild type, single mutants *rnf-5(tm794)* and *ire-1(v33)* and double mutants *rnf-5(tm794);ire-1(v33)*. (B) Bar graph showing the mean fluorescence (arbitrary units [AU]) measured in the anterior intestine. Four independent experiments were performed with n ≥ 40 in each genetic background. Values are the mean ± SE. Statistical significance was calculated by one-way ANOVA $F(3,76)=293.7$, P value < 0.0001, followed by Tukey's multiple comparisons test $p<0.04$ (*), $p<0.0004$(**), and $p<0.0001$ (***).

Table S1. Two-way ANOVA analysis followed by Post-Hoc Bonferroni-corrected test for Fig. 1C.

Condition	**Genotype**	**% L4 and adult** **(mean ± SE)**	**p-value relative to *rnf-5(tm794);ire-1(v33)***
DMSO	N2 *rnf-5(tm794)* *ire-1(v33)* *rnf-5(tm794);ire-1(v33)*	91.9 ± 1.2 91.1 ± 1.4 69.7 ± 2.6 80.9 ± 2.4	0.000126 0.000782 0.002362
Tunicamycin (1 µg/ml)	N2 *rnf-5(tm794)* *ire-1(v33)* *rnf-5(tm794);ire-1(v33)*	76.6 ± 2.3 89.2 ± 1.7 60.3 ± 3.5 72.3 ± 3.1	0.3 0.000042 0.0162

Table S2. L1 survival analysis at 20˚ (related to Fig. 2A-D).

Exp. No.	Genotype	Mean survival (days)	p-value relative to N2*	p-value relative to *ire-1(v33)* *	p-value relative to *rnf-5(tm794);ire-1(v33)* *	Events	Comments
1	N2	19±0.3				403	
	rnf-5(tm794)	18.4±0.3	0.7099		<0.0001	520	
	atg-3(bp412)	7.8±0.2	<0.0001			499	
	ire-1(v33)	7.6±0.5	<0.0001		0.0013	444	
	rnf-5(tm794);ire-1(v33)	10.9±0.5	<0.0001	0.0013		312	
	atg-3(bp412);ire-1(v33)	5±0.3	<0.0001	<0.0001		263	
	atg-3(bp412);rnf-5(tm794)	8.9±0.2	<0.0001			481	
	atg-3(bp412);rnf-5(tm794);ire-1(v33)	7.2±0.2	<0.0001	0.0842	<0.0001	438	
2	N2	21.8±0.2				472	Figure 2
	rnf-5(tm794)	23.3±0.2	<0.0001		<0.0001	472	
	atg-3(bp412)	11.6±0.2	<0.0001			418	
	ire-1(v33)	10.2±0.5	<0.0001		<0.0001	337	
	rnf-5(tm794);ire-1(v33)	15.2±0.3	<0.0001	<0.0001		471	
	atg-3(bp412);ire-1(v33)	7.9±0.3	<0.0001	<0.0001		346	
	atg-3(bp412);rnf-5(tm794)	12.5±0.3	<0.0001			500	
	atg-3(bp412);rnf-5(tm794);ire-1(v33)	9.4±0.4	<0.0001	0.0096	<0.0001	328	
3	N2	16.2±0.2				526	
	rnf-5(tm794)	18.2±0.2	<0.0001		<0.0001	370	
	atg-3(bp412)	9.7±0.2	<0.0001			490	
	ire-1(v33)	N.D.	N.D.			N.D.	
	rnf-5(tm794);ire-1(v33)	9.5±0.3	<0.0001			563	
	atg-3(bp412);ire-1(v33)	7.3±0.3	<0.0001			345	
	atg-3(bp412);rnf-5(tm794)	9.4±0.1	<0.0001			576	
	atg-3(bp412);rnf-5(tm794);ire-1(v33)	7.8±0.2	<0.0001		<0.0001	685	
4	N2	12±0.3				534	
	rnf-5(tm794)	14±0.5	<0.0001		<0.0001	397	
	atg-3(bp412)	6.8±0.2	<0.0001			425	
	ire-1(v33)	5.5±0.3	<0.0001		0.0154	327	
	rnf-5(tm794);ire-1(v33)	6.5±0.4	<0.0001	0.0154		320	
	atg-3(bp412);ire-1(v33)	4.7±0.3	<0.0001	0.0355		298	
	atg-3(bp412);rnf-5(tm794)	6.1±0.2	<0.0001			536	
	atg-3(bp412);rnf-5(tm794);ire-1(v33)	6.4±0.2	<0.0001	0.0225	0.2362	705	

Results of four L1 survival experiments.

*Statistical analysis was calculated using Log-Rank test (OASIS).

Table S3. Lifespan analysis at 20˚ (related to Fig. 3A-D).

exp. no.	genotype	mean lifespan (days)	p-value relative to N2 *	p-value relative to *ire-1(v33)* *	p-value relative to *rnf-5(tm794);ire-1(v33)* *	events/ observations	comments
1	N2	20±0.5				98/120	Figure 3
	rnf-5(tm794)	21.1±0.5	0.0635		<0.0001	100/120	
	atg-3(bp412)	13.9±0.2	<0.0001			83/120	
	ire-1(v33)	9.4±0.3	<0.0001		<0.0001	110/120	
	rnf-5(tm794);ire-1(v33)	12.5±0.3	<0.0001	<0.0001		106/120	
	atg-3(bp412);ire-1(v33)	9.7±0.2	<0.0001	0.7015		79/120	
	atg-3(bp412);rnf-5(tm794)	14.1±0.2	<0.0001			112/120	
	atg-3(bp412);rnf-5(tm794);ire-1(v33)	10.5±0.3	<0.0001	0.2271	<0.0001	93/120	
2	N2	19.8±0.5				83/120	
	rnf-5(tm794)	20.8±0.4	0.4020		<0.0001	84/120	
	atg-3(bp412)	14.9±0.4	<0.0001			81/120	
	ire-1(v33)	11.5±0.3	<0.0001		<0.0001	94/120	
	rnf-5(tm794);ire-1(v33)	14.1±0.2	<0.0001	<0.0001		90/120	
	atg-3(bp412);ire-1(v33)	10.5±0.2	<0.0001	0.0002		95/120	
	atg-3(bp412);rnf-5(tm794)	15.2±0.3	<0.0001			60/120	
	atg-3(bp412);rnf-5(tm794);ire-1(v33)	11.7±0.2	<0.0001	0.3172	<0.0001	83/120	
3	N2	19.9±0.4				91/120	
	rnf-5(tm794)	21±0.5	0.0146		<0.0001	88/120	
	atg-3(bp412)	14.2±0.3	<0.0001			97/120	
	ire-1(v33)	9.5±0.3	<0.0001		<0.0001	105/120	
	rnf-5(tm794);ire-1(v33)	13.1±0.4	<0.0001	<0.0001		95/120	
	atg-3(bp412);ire-1(v33)	8.1±0.3	<0.0001	<0.0001		85/120	
	atg-3(bp412);rnf-5(tm794)	15±0.3	<0.0001			104/120	
	atg-3(bp412);rnf-5(tm794);ire-1(v33)	11.7±0.2	<0.0001	0.0012	<0.0001	91/120	

The results of three lifespan experiments.

*Statistical analysis was calculated using Log- Rank test (OASIS)

Table S4. Differentially expressed proteins identified in the proteomics screen of *rnf-5(tm794)* and wild
The experimental group carrying the rnf-5(tm794) allele was grown on ^{15}N labeled bacteria
(H).

sequence	Gene Name	Description	
Y56A3A.3	*mif-1*	MIF (Macrophage migration Inhibitory Factor) related	intestine,
K08D10.3	*rnp-3*	RNP (RRM RNA binding domain) containing	
H27M09.2	*rpb-5*	RNA Polymerase II (B) subunit	
F57F5.1	*F57F5.1*	cysteine-type peptidase (ortholog of cathepsin B)	predicted:
C17F4.7	*C17F4.7*	unknown	intestine,p
F58B3.1	*lys-4*	LYSozyme	predicted:
F58B3.3	*lys-6*	LYSozyme	predicted:
T13B5.3	*pho-14*	intestinal acid PHOsphatase	intestine,
C04G2.6	*dis-3*	DIS3 (yeast disjunction abnormal) exonuclease homolog	pharynx, m system, co
Y43F8C.13	*Y43F8C.13*	predicted purine nucleosidase	intestine,p
C52E4.1	*cpr-1*	Cysteine PRotease related	intestine
T21H3.1	*T21H3.1*	hydrolase	intestine
T21G5.3	*glh-1*	Germ Line Helicase	germline
C55B7.1	*glh-2*	Germ Line Helicase	germline
H20J04.4	*H20J04.4*	DEAD-box RNA helicase	
F53G2.6	*tsr-1*	Transporter of SR proteins	
H37A05.1	*lpin-1*	LIPIN (mammalian lipodystrophy associated) homolog	vulval mus
T04H1.9	*tbb-6*	TuBulin, Beta	pharynx
R05F9.8	*msp-33*	Major Sperm Protein	primary sp
F47B10.2	*haly-1*	Histidine Ammonia LYase	nervous sy
F27D4.4	*F27D4.4*	zinc finger CCCH-type	intestine,
F43D9.4	*sip-1*	Stress Induced Protein	
D1054.8	*D1054.8*	dehydrogenase	
H13N06.6	*tbh-1*	Tyramine Beta Hydroxylase	nervous sy
R05G6.7	*vdac-1*	VDAC (Voltage Dependent Anion Channel) homolog	muscle, hy
R10E9.1	*msi-1*	MuSashi (fly neural) family	nervous sy
F40F4.6	*irg-7*	Infection Response Gene	intestine
C04F6.1	*vit-5*	VITellogenin structural genes (yolk protein genes)	intestine
F59D8.1	*vit-3*	VITellogenin structural genes (yolk protein genes)	intestine
F59D8.2	*vit-4*	VITellogenin structural genes (yolk protein genes)	
K10C2.3	*asp-14*	ASpartyl Protease	
C39D10.7	*C39D10.7*	chitin-binding protein	reproducti
D1037.3	*ftn-2*	FerriTIN	intestine,
F25D7.4	*maph-1.2*	Microtubule-Associated Protein Homolog	
C36A4.5	*maph-1.3*	Microtubule-Associated Protein Homolog	

C28C12.7	*spp-10*	SaPosin-like Protein family	intestine, r
F44C4.3	*cpr-4*	Cysteine PRotease related	intestine
Y37A1B.17	*Y37A1B.17*	guanine nucleotide exchange factor	
F37C12.13	*exos-9*	EXOSome (multiexonuclease complex) component	muscle, ge
C25B8.3	*cpr-6*	Cysteine Protease related	
H15N14.1	*adr-1*	Adenosine Deaminase acting on RNA	nervous sy
F18A1.5	*rpa-1*	Replication Protein A homolog	pharynx, g
F21F8.7	*asp-6*	ASpartyl Protease	intestine, p
T05C3.5	*dnj-19*	DNaJ domain (prokaryotic heat shock protein)	
R08E5.3	*R08E5.3*	methyltransferase	intestine
K12G11.3	*sodh-1*	Sorbitol DeHydrogenase family	intestine, r
F56C9.10	*F56C9.10*	microtubule associated cell migration factor	muscle, ne
K07C11.2	*air-1*	Aurora/Ipl1 Related kinase	germline, d